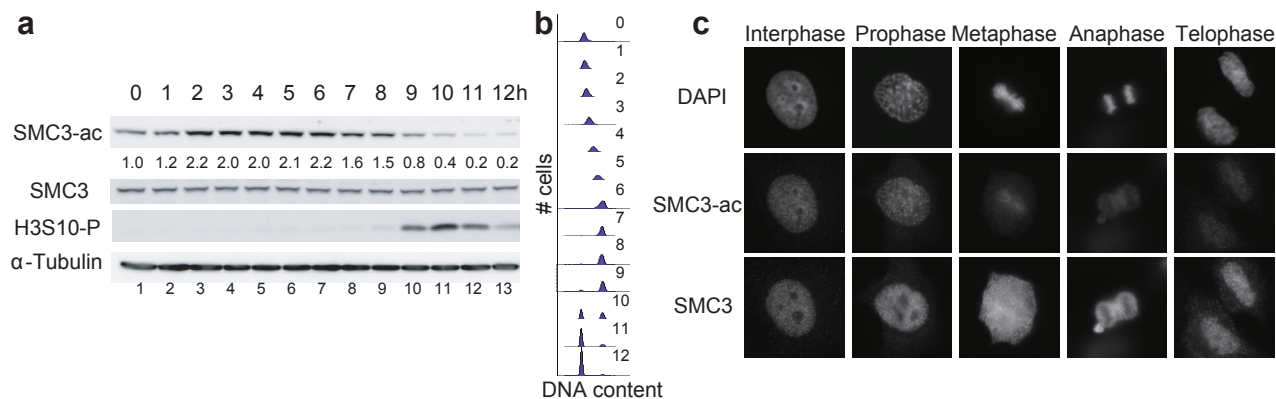


SUPPLEMENTARY INFORMATION



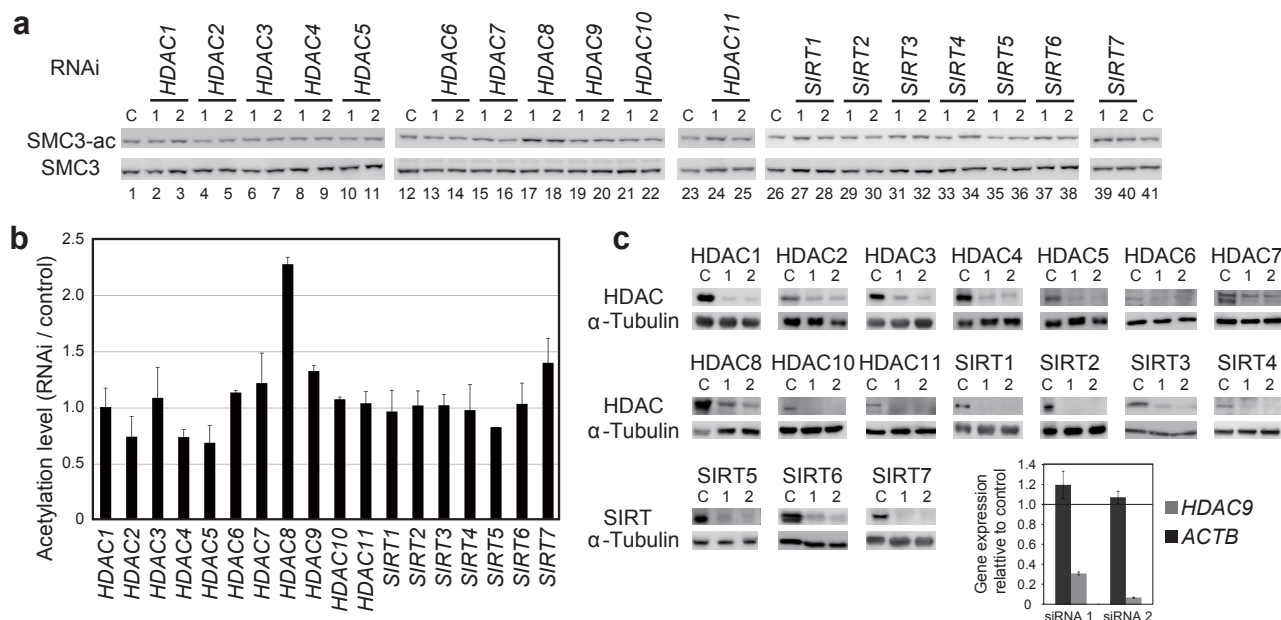
Supplementary Figure 1 | Vertebrate SMC3 demonstrates cell cycle-regulated acetylation.

a, HeLa cells were synchronized in early S-phase using a double thymidine arrest and total cell extracts were prepared at the indicated time points after release. Levels of acetylated SMC3 (SMC3-ac), total SMC3, Histone H3 Serine 10 phosphorylation (H3S10-P; a metaphase marker), and α-Tubulin were assessed by SDS-PAGE and immunoblotting. Numbers beneath SMC3-ac bands indicate quantification of SMC3-ac levels normalized to SMC3 levels and the 0 hour time point.

b, FACS analysis of cell cycle distribution for cells in panel (a).

Although total SMC3 levels remain stable throughout the cell cycle, SMC3 is increasingly acetylated during S-phase and peaks during G2 (5-6 h post-release). This is accompanied by a marked decline in SMC3-ac during mitosis. There is no evidence of SMC3 destruction, consistent with a role for coordinated deacetylation.

c, Immunostaining of acetylated SMC3 nuclear localization. Cells were prepared as in (a), fixed with paraformaldehyde and immunostained for acetylated SMC3 (SMC3-ac), total SMC3, and DNA (DAPI). This data shows that SMC3-ac localizes within the nucleus during interphase and remains chromatin-bound until metaphase, when the bulk of SMC3 is released. These data suggest that SMC3 acetylation is tightly regulated to coordinate SMC3-binding to chromosomes at specific times of the cell cycle.



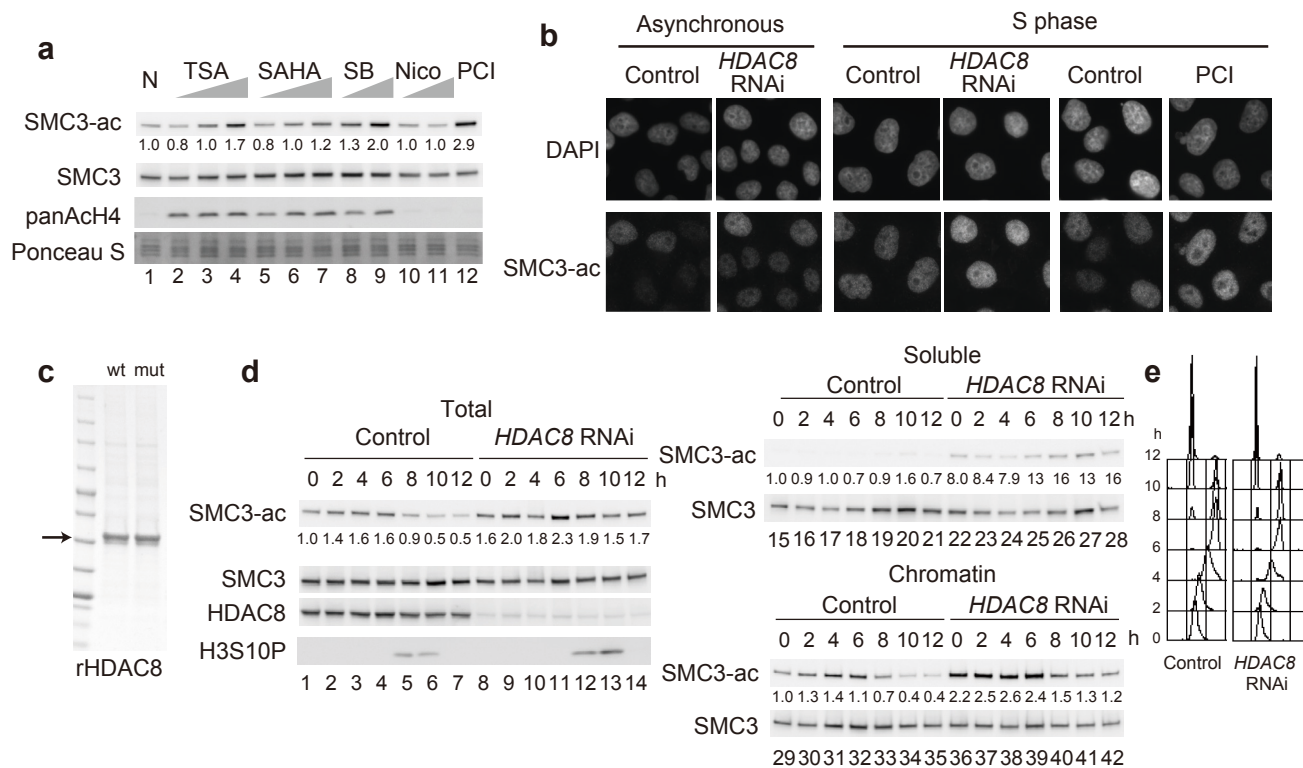
Supplementary Figure 2 | Vertebrate SMC3 is deacetylated by HDAC8.

a, Identification of an SMC3 deacetylase by RNAi-based screening. Cell extracts were prepared from unsynchronized HeLa cells after transfection with the indicated siRNAs for each human deacetylase (HDAC1-11 or SIRT1-7). Acetylation status of SMC3 was analyzed by western blotting using an anti-SMC3-ac antibody. Total levels of SMC3 served as a loading control. In each knock down experiment, two independent siRNA sequences were used ("1" and "2"). Total cell lysates were prepared 48 hours after transfection and the levels of acetylated SMC3 (SMC3-ac) and SMC3 were analyzed by SDS-PAGE and immunoblotting. "C" indicates sample with transfection of control siRNA.

b, SMC3 acetylation levels in panel (a) were normalized to that of control cells. The average acetylation levels and standard deviation for two independent siRNAs are shown.

c, Western blotting of samples in panel (a) was performed with available antibodies for HDACs, SIRT proteins and α -Tubulin to assure knockdown of each deacetylase. Since antibodies were not available for HDAC9, the efficiency of knock down was determined by RT-PCR. Error bars represent standard deviations.

Knockdown of HDAC8 resulted in the most consistent increase of SMC3-ac.



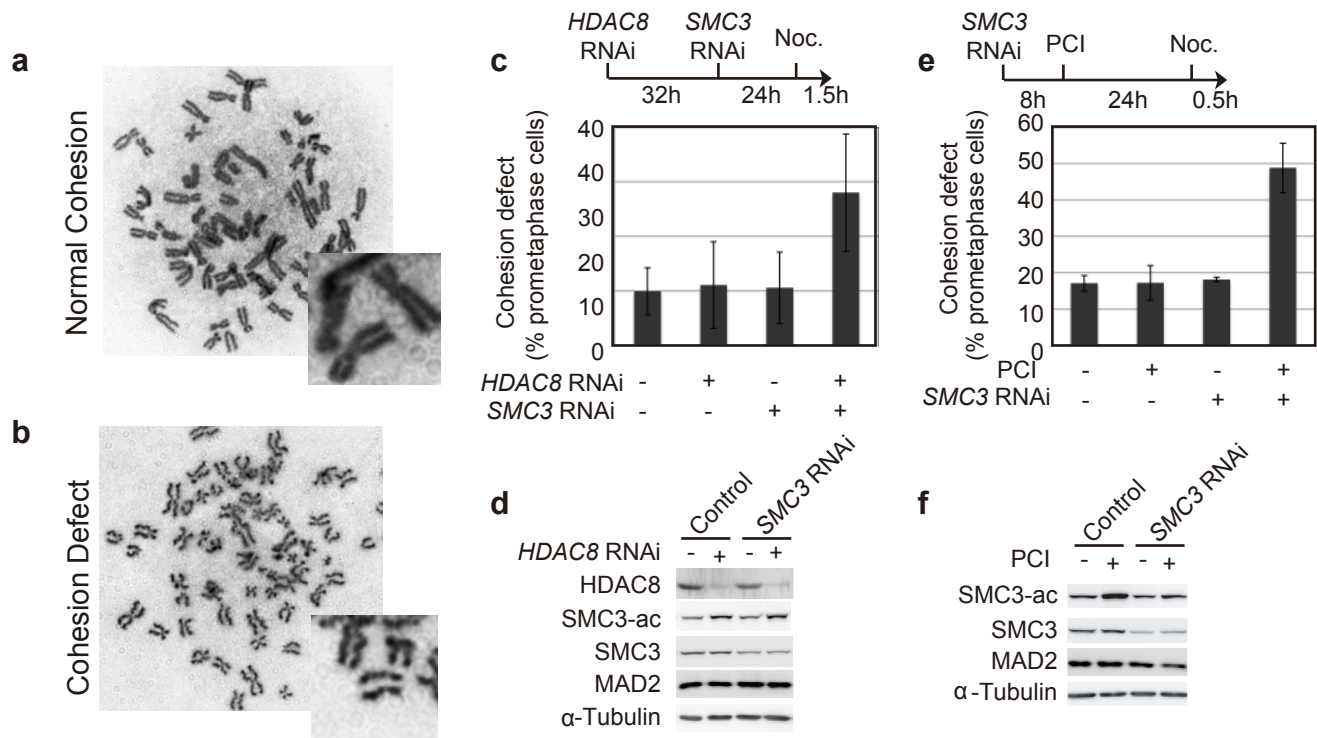
Supplementary Figure 3 | Chromatin localization of SMC3-ac depends on HDAC8 activity.

a, HDAC8 inhibition by histone deacetylase inhibitors. HeLa cells were treated with increasing concentration of Trichostatin A (TSA; 0.5, 1, 2 μ M), suberoylanilide hydroxamic acid (SAHA; 5, 10, 20 μ M), sodium butyrate (SB; 10, 50 mM), nicotinamide (Nico; 2, 10 mM), PCI-34051¹ (25 μ M), or water (N) for 4 h. Cell extracts were prepared and levels of acetylated SMC3 (SMC3-ac), SMC3, and acetylated histone H4 (panACh4) were analyzed by SDS-PAGE and immunoblotting. PCI treatment results in a strong increase of SMC3-ac without any detectable H4 acetylation.

b, Unsynchronized HeLa cells were transfected with HDAC8 siRNA for 48 h (left), or synchronized in S-phase by culturing for 6 h after release from double thymidine arrest (center), or treated with 25 μ M PCI for 6 hrs (right). The cells were fixed with 4% paraformaldehyde and immunostained for SMC3-ac and DNA (DAPI). HDAC8 RNAi in asynchronous and synchronous cells, as well as PCI treatment increases SMC3-ac.

c, Purified wild type (wt) and mutant (mut) recombinant HDAC8 protein from baculovirus-infected Sf9 cells was separated by SDS-PAGE and stained by Coomassie brilliant blue (CBB).

d, HeLa cells were transfected by HDAC8 siRNA or control siRNA for 48 h. Cells were synchronized by double thymidine arrest and released for the indicated time. Cell extracts were fractionated into soluble and chromatin fractions. The levels of acetylated SMC3 (SMC3-ac), SMC3, HDAC8, α -Tubulin, and phosphorylated Histone H3 at Serine 10 (H3S10-P), were analyzed by SDS-PAGE and immunoblotting. **e**, Cell cycle progression was analyzed by FACS.



Supplementary Figure 4 | Role of HDAC8 activity on sister chromatid cohesion.

Representative images of metaphase spreads from HDAC8- and SMC3-depleted cells. Individual chromosomes are shown at higher magnification in the right lower inset. Cohesion was considered normal if sister chromatids were tightly connected at their centromeres (**a**). Metaphases that lacked primary constrictions and in which sister chromatids were abnormally spaced for a majority of chromosomes were considered to have cohesion defects (**b**).

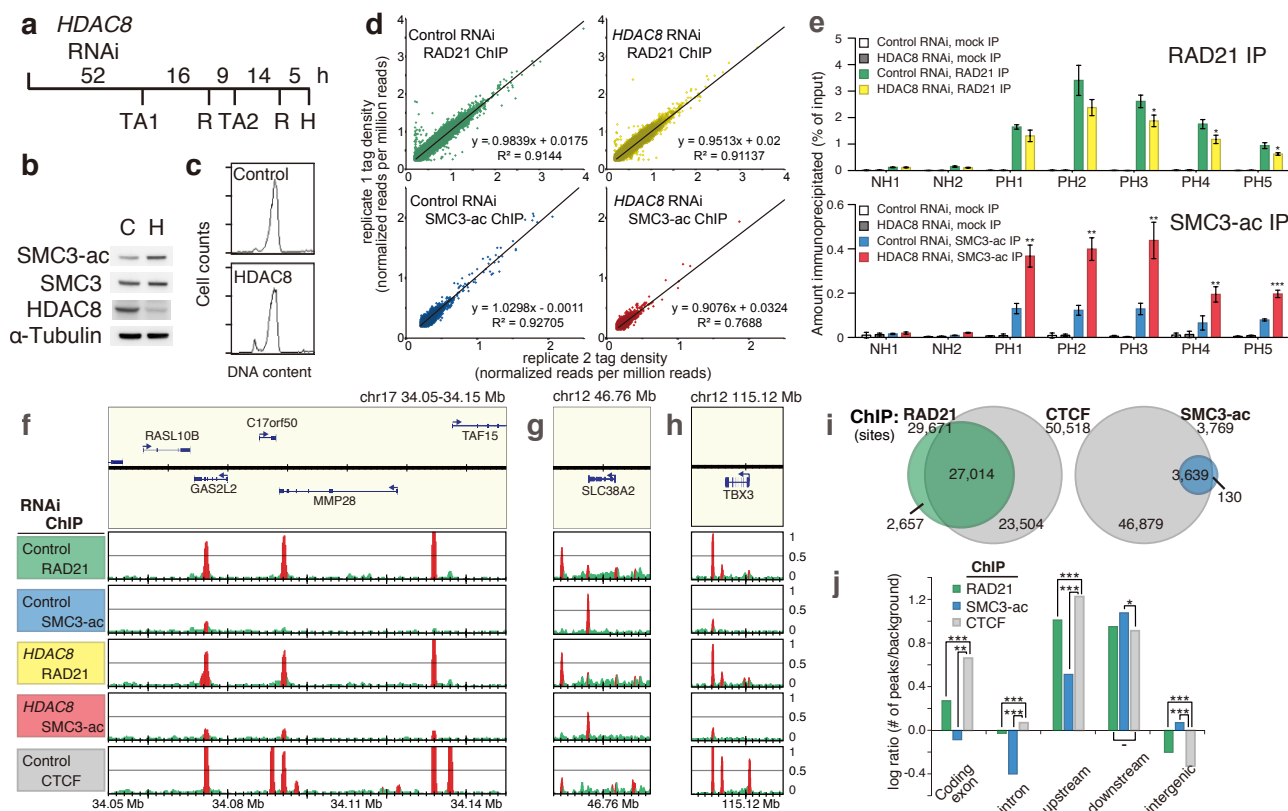
c, HeLa cells were transfected with HDAC8 siRNA and 32 h later transfected with SMC3 siRNA. The cells were cultured for 24 h and incubated with nocodazole for 1.5 h. The mitotic cells were collected by shake-off and analyzed by hypotonic spreading and Giemsa staining. The frequency of cohesion defects was assessed as in (**a**) and (**b**). For each condition, 110-180 metaphases were assessed and bars represent standard deviations for duplicate experiments.

d, The levels of HDAC8, acetylated SMC3 (SMC3-ac), SMC3, MAD2, and α -Tubulin were analyzed for cells in panel (**c**) by SDS-PAGE and immunoblotting.

e, HeLa cells were transfected with SMC3 siRNA and 8 h later were cultured in the presence or absence of PCI for 24 h. After 0.5 h treatment by nocodazole, the mitotic cells were collected and analyzed as in (**c**).

f, The levels of acetylated SMC3 (SMC3-ac), SMC3, MAD2 and α -Tubulin for cells analyzed in panel (**e**).

We observed few sister-chromatid cohesion defects after 48 h of transfection with HDAC8 siRNA alone. However, with concurrent reduction of SMC3 by co-transfection of SMC3 siRNA, we observed that 28% of cells defects in sister-chromatid cohesion (**c**). This effect was not a result of depletion of the spindle assembly checkpoint component MAD2, which has been shown to result from off-target effects of RNAi and lead to artefactual loss of sister chromatid cohesion^{2,3} (**d,f**). This effect was reproducible with the concurrent use of the HDAC8 inhibitor PCI in combination with SMC3 siRNA (**e,f**), resulting in cohesion defects in 48% of cells.



Supplementary Figure 5 | Supplementary data for ChIP-Seq from HeLa cells.

a, Schematic representation of the experimental protocol of the cells for ChIP-seq. HeLa cells were transfected with control or *HDAC8* RNAi for 52 h prior to G1/S-phase synchronization using a double thymidine arrest (TA). Cells were subsequently released (R) and harvested (H) in late S/early G2 phase after 5 h of growth, the time when overall SMC3-ac as well as chromatin-bound SMC3-ac reaches a maximum level (Fig. 1e, Supplementary Figs 1a and 3d).

b, The levels of SMC3-ac, SMC3 and HDAC8 in cells from (a) used for ChIP-Seq as analyzed by immunoblotting. Alpha-tubulin is used as a protein loading control. HDAC8 levels are strongly diminished and SMC3-is increased.

c, FACS analysis of treated cells from (a) shows the majority of cells in S/G2.

d, Regression analysis of replicate ChIP-Seq experiments. Each dot represents one localization peak shared between the replicate experiments with two axes representing the tag intensity for each replicate. The equation describing linear fit and correlation (R^2) is indicated for each.

e, ChIP qPCR verification of binding sites identified by HeLa cell ChIP-Seq. ChIP DNA using RAD21 and SMC3-ac antibodies was analyzed by qPCR using 2 pairs of primers for negative sites (NH1,2) and 5 pairs of primers for sites showing increased binding for SMC3-ac (PH1-5). Error bars represent standard deviation. Significance by two-tailed paired t-test are indicated by * ($p < 0.05$), ** ($p < 0.01$) and *** ($p < 0.001$).

Additional examples of RAD21, SMC3-ac and CTCF localization sites for control and *HDAC8* RNAi-treated HeLa cells on chromosomes 17 (f), and 12 (g, h).

i, Comparison of CTCF to RAD21 and SMC3-ac localization sites in HeLa cells. This data shows that 53% of CTCF sites overlap with RAD21, but only 7% of CTCF sites overlap SMC3-ac localization peaks.

j, Distribution of CTCF binding sites compared to RAD21 and SMC3-ac sites. CTCF sites are significantly enriched with respect to RAD21 and SMC3-ac in the upstream, coding exons and introns of genes, less enriched in intergenic regions compared with RAD21 and SMC3-ac and less enriched than SMC3-ac downstream of genes. The data from (h) and (i) demonstrate overlapping but different distributions suggest that the function of CTCF and acetylation on cohesin may differ.

Along with data in Fig. 2, these results indicate that altered cohesin acetylation does not result in ectopic localization sites (Fig. 2a-c, and f-h above), with more than 95% of threshold-meeting peaks for SMC3-ac overlapping with RAD21 in both control and *HDAC8* depleted cells, and nearly 93% of RAD21 peaks in the *HDAC8*-reduced cells overlapping those in control cells. Furthermore, despite a smaller number of threshold-meeting peaks, nearly 60% of SMC3-ac peaks overlapped in both control and *HDAC8* RNAi-treated cells (Fig. 2a-c). ChIP-qPCR analyses of candidate binding sites selected for increased SMC3-ac binding were able to confirm the findings noted by ChIP-Seq (e, above).

Supplementary Figure 6 |
Supplementary data for HDAC8
mutations in CdLS.

a. Monoallelic Expression of HDAC8 mutations. Chromatograms demonstrating the mutation for each proband, available family members and available cDNAs are indicated with the mutation in each family aligned in a boxed column labeled with the study identifier and mutation at the top. Unless labeled otherwise, samples are from peripheral blood genomic DNA. The arrow at the bottom denotes the mutated nucleotide. Note that female probands and carrier mother demonstrate equal levels of mutated and normal alleles in peripheral blood DNA. Available lymphoblastoid cell lines from two female probands (CDL016 and CDL248) demonstrate expression of the normal allele only, even when grown in the presence of 1mg/ml cycloheximide. Fibroblasts from proband CDL016 demonstrate expression of only the mutated allele. As expected, the male probands demonstrate hemizygous mutations in peripheral blood and express only this allele in cell lines. These results are consistent with selection against HDAC8 mutations in the peripheral blood for this X-linked Lyonized gene⁴.

b. FACs analysis of Control and HDAC8 p.G320R mutant LCLs shows similar cell cycle profile, largely in G1.

c. Conservation of mutated HDAC8 residues. Clustal W alignments of HDAC8 homologs are labeled with species and corresponding protein name at the left. Dark grey boxes represent identical residues when compared to the human protein. Light grey shaded boxes indicate similar residues. Mutation residue positions using human numbering are indicated above and denoted by orange boxes. Each mutation is also predicted to be detrimental to protein function by SIFT⁵ and PolyPhen⁶.

d. The H180R mutation disrupts coordination of the catalytic zinc ion (Zn), while the T311M mutation could perturb interactions with the loop containing the catalytically important residue Y306.

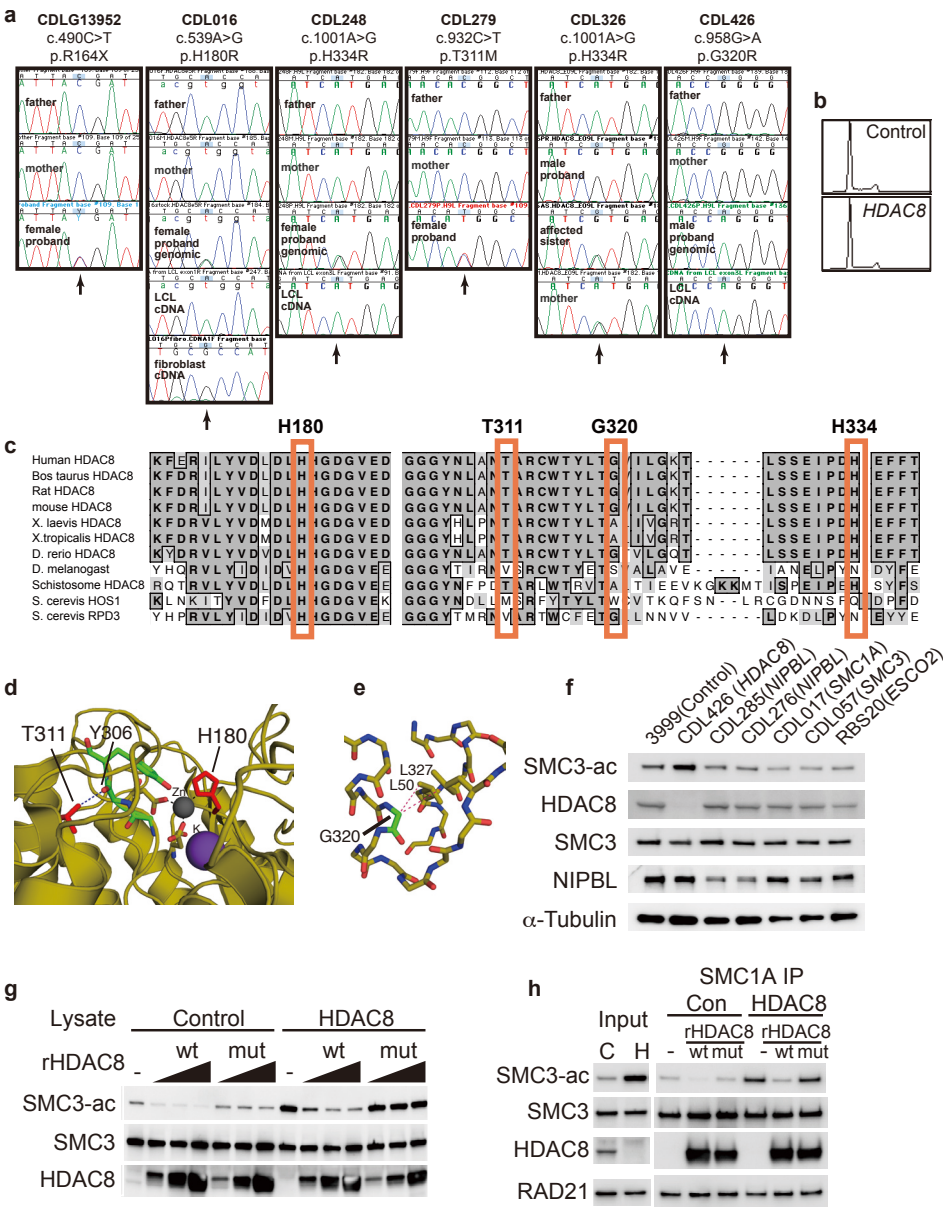
e. The Cα atom of G320 packs closely against adjacent leucine residues, as indicated by the dotted red lines, and the large, positively charged side chain of arginine in the G320R mutant would disrupt these packing interactions and lead to significant structural rearrangements.

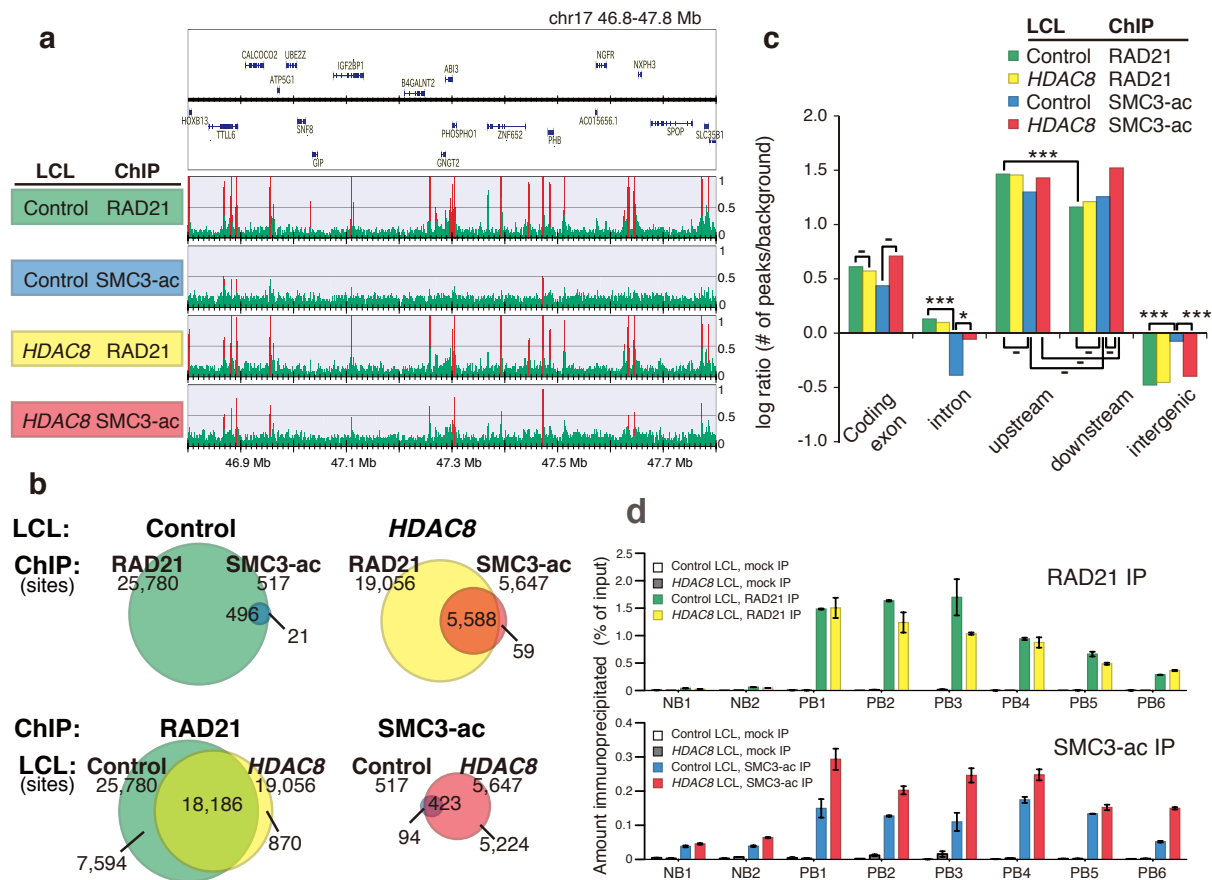
f. Immunoblotting analysis (SMC3-ac, HDAC8, SMC3, NIPBL, and α-Tubulin) of total extracts from Cohesinopathy individual-derived LCLs. No LCLs derived from probands with mutations in NIPBL, SMC1A, SMC3 or ESCO2, show no significant alteration of SMC3-ac or HDAC8 levels.

To further ensure that loss of HDAC8 activity is the cause of increased SMC3-ac in the patients' cells (Fig. 3b), we tested LCL lysates (g) as well as immunopurified cohesin complex (h) from control and HDAC8-mutant LCLs (p.G320R) to assess whether purified wild type and catalytically inactive recombinant HDAC8 from baculovirus could rescue this defect.

g. Total cell extracts from Control- and HDAC8-mutant LCLs were incubated with increasing concentrations of wild type (wt) mutant (mut) recombinant HDAC8 (rHDAC8) protein and rHDAC8 mutant proteins at 30C for 1h and analyzed by SDS-PAGE and immunoblotting.

h. SMC1A-containing cohesin complex was immunopurified from Control- and HDAC8-mutant LCL extracts and incubated with rHDAC8 and rHDAC8 mutant protein at 30C for 1h and assayed as in (g).

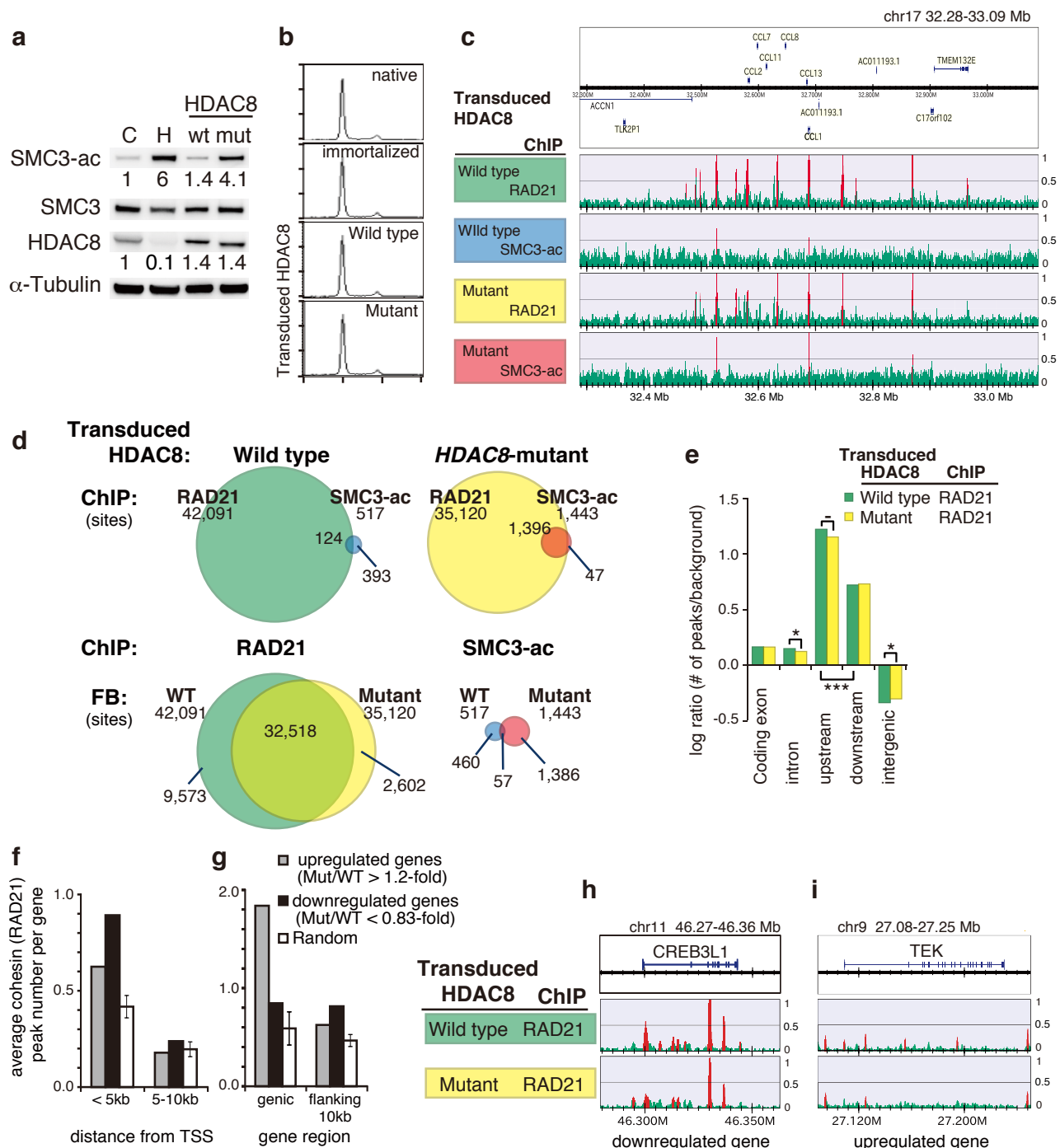




Supplementary Figure 7 | HDAC8-mutant LCL ChIP-Seq analysis.

a, Binding profiles for RAD21 and acetylated SMC3 in control and HDAC8-mutant LCLs. **b**, Venn diagrams showing overlap of localization sites. **c**, Classification of RAD21 and SMC3-ac localization sites as a log ratio to background reads. Significance was calculated using a 2-sample test for equality of proportions; *, **, *** and -, indicate $p < 0.05$, $p < 0.001$, $p < 0.0001$ and $p > 0.05$, respectively. "Upstream" and "downstream" are defined as within 5kb from 5' and 3' transcript gene boundaries, respectively. **d**, ChIP qPCR verification of binding sites identified by LCL ChIP-Seq. ChIP DNA using RAD21 and SMC3-ac antibodies was analyzed by qPCR using 2 pairs of primers for negative sites (NB1,2) and 6 pairs of primers for positive sites (PB1-6). Error bars represent standard deviations.

Using unsynchronized growth conditions, these cultures demonstrated similar cell cycle progression (Supplementary Fig. 6b), and notably increased levels of total SMC3-ac (Supplementary Fig. 6g,h). Like the observations for HDAC8 RNAi treatment of HeLa cells, we noted a >96% overlap of SMC3-ac sites with RAD21 sites, and a 95% overlap of RAD21 sites in control and HDAC8 LCLs (b). In contrast to HeLa cell experiments where SMC3-ac levels were maximized using cell cycle synchronization to late S/G2, which maximized chromatin binding in both control and test cells, we noted few SMC3-ac localization sites in unsynchronized control LCLs, consistent with the predominance of cells in G1 (Supplementary Fig. 6b). We also noted dramatically more SMC3-ac localization sites in HDAC8-mutant LCLs, consistent with the marked increase of total SMC3-ac in these cells, likely caused by this functionally near-null mutation, as suggested by immunoblotting. The finding of a significant amount of chromatin-bound acetylated cohesin, despite cells being predominantly in G1, suggests that acetylated cohesin is being reloaded and is capable of localizing appropriately. Although there were insufficient SMC3-ac localization sites in control LCLs to statistically detect binding region changes for SMC3-ac, we noted similar trends in distribution as seen in S/G2 synchronized HeLa cells.



Supplementary Figure 8 | Analysis of Cohesin (RAD21) and SMC3-ac localization and transcription in wild type or mutant HDAC8-rescued HDAC8-mutant CdLS fibroblasts.

a, Immortalized HDAC8 p.H180R-mutant fibroblasts were transduced by lentiviral vector expressing either wild type (wt) or catalytically inactive HDAC8 (mut). Levels of SMC3-ac, SMC3, HDAC8 and α-Tubulin were analyzed by immunoblotting. Numbers beneath lanes indicate quantification of levels compared with control (C) fibroblasts.

b, FACS analysis of fibroblast cell lines. Native, untransformed fibroblasts expressing the mutant p.H180R allele (top), were transformed with hTERT (immortalized) and subsequently transduced with either wild type or mutant HDAC8. DNA content is on the X-axis and cell number on the Y-axis.

c, Example of Fibroblast ChIP-seq data (position 32.28 – 33.09 Mb of human chromosome 17). ChIP-Seq data are shown in reads per million. Regions with significant enrichment (see Methods) are colored in red. Localization profiles for cohesin (RAD21) and acetylated SMC3 (SMC3-ac) in HDAC8 p.H180R-mutant fibroblasts expressing either wild type HDAC8 (wt) and catalytically inactive HDAC8 (mut) are shown.

d, Venn diagrams showing overlap of binding sites. Numbers of total sites and overlapping sites are indicated for each condition.

e, Classification of RAD21 and SMC3-ac localization sites as a log ratio to background reads. Significance was calculated using a 2-sample test for equality of proportions; *, **, *** and -, indicate $p < 0.05$, $p < 0.001$, $p < 0.0001$ and $p > 0.05$, respectively. "Upstream" and "downstream" are defined as 5kb from gene boundaries, respectively. **f-i**, Correlation between transcriptional alteration and cohesin/RAD21 localization with loss of HDAC8 activity. **f**, Transcriptionally altered genes show loss of cohesin binding near their transcription start sites (TSS). Genes that are upregulated (Mut/WT > 1.2 fold, grey, n=56 genes) or downregulated (Mut/WT < 0.83 fold, black, n=130 genes) due to loss of HDAC8 have a increase of cohesin binding sites within 5kb of their TSS compared sites 5-10kb from the TSS. Data is shown for cohesin/RAD21 localization sites in the fibroblasts expressing wild type HDAC8; the results using mutant HDAC8 were proportionately identical, but ~16% less for each category (the same rate as overall cohesin binding). **g**, The upregulated genes have a loss of cohesin/RAD21 localization sites within the gene compared with regions 0-10kb outside the gene. The y-axis indicates the average number of binding sites per dysregulated gene in the mutant cells. Randomly picked genes (white, mean \pm S.D., using 8,000 sets of 130 genes) serve as a control reference. Examples of reduced RAD21 localization sites in **(h)** a down-regulated gene (*CREB3L1*) and **(i)** an up-regulated gene (*TEK*) in control and mutant.

To determine the effect of HDAC8 loss on cohesin localization and its concurrent effect on transcription we wished to minimize abnormal chromosomal regulation and expression variation. We wanted to perform these studies in a relatively normal cell line, as opposed to one derived from cancer, and wanted them to be performed on an isogenic background, which is difficult using LCLs. Hence, we utilized the fibroblasts from one of the girls that are Lyonized to express only the enzymatically inactive HDAC8 p.H180R mutation. Following immortalization by constitutive expression of hTERT, we co-expressed either wild type or catalytically inactive HDAC8. The cell lines expressed wild type or mutant HDAC8 at similar levels comparable to that of a control fibroblast cell line (a). With ChIP-Seq analysis of unsynchronized cells, largely in G1 (b), with low levels of SMC3-ac we again noted only low number of SMC3-ac sites. Nonetheless, we again observed a 16% overall decrease in RAD21/cohesin localization sites, a nearly 3-fold increase of SMC3-ac sites in HDAC8-mutant cells, a 97% overlap of SMC3-ac with RAD21 sites in HDAC8-mutant cells and a 93% overlap of cohesin sites in the mutant lines with that of wild type (c,d). As in the LCL experiments, the extremely low level of SMC3-ac binding in wild type cells results in a high background to signal ratio for the experiment (c) and disrupts the ability to statistically evaluate both the overlap of these sites and their correlation with transcription (below). Nonetheless, we again noted consistent enrichment of RAD21 at regions within 5kb upstream/downstream of ORFs⁷⁻¹⁰ (e). These data correlate nearly identically with that observed in HeLa and LCL experiments to strongly support the model that constitutive reduction of HDAC8 activity allows grossly normal cohesin localization but results in the association of unstable cohesin containing residual acetylated SMC3-containing cohesin with chromosomes, subsequently reducing the overall number of functional cohesin complexes.

To further understand functional relationships between HDAC8 and transcriptional regulation, we analyzed expression by RNA-Seq on the same cells assessed by ChIP-Seq. As in LCLs, the transcriptional changes are not of large magnitude and only 56 or 130 genes are significantly increased and decreased, respectively, in the cell line that expresses inactive HDAC8 (Supplementary Tables 8 and 9). Most changes are within 1.5 fold, consistent with the small changes noted for *NIBPL* mutations in other settings^{7,11-13}. We identified several correlations between cohesin localization sites and genes with transcriptional status altered by loss of HDAC8. We noted a general increase of cohesin binding sites within 5kb of the transcription start site (TSS) for genes that are both positively and negatively altered by loss of HDAC8 activity (f). We also noted that loss of HDAC8 activity correlates with upregulation of genes with cohesin sites within the gene (g). Two examples are illustrated (h,i) that include *CREB3L1*, where loss of cohesin sites near the TSS (5' of ORF) causes down regulation and *TEK*, where cohesin loss within the gene results in upregulation.

Supplementary Figure 9 | HDAC8 and cohesin recycling

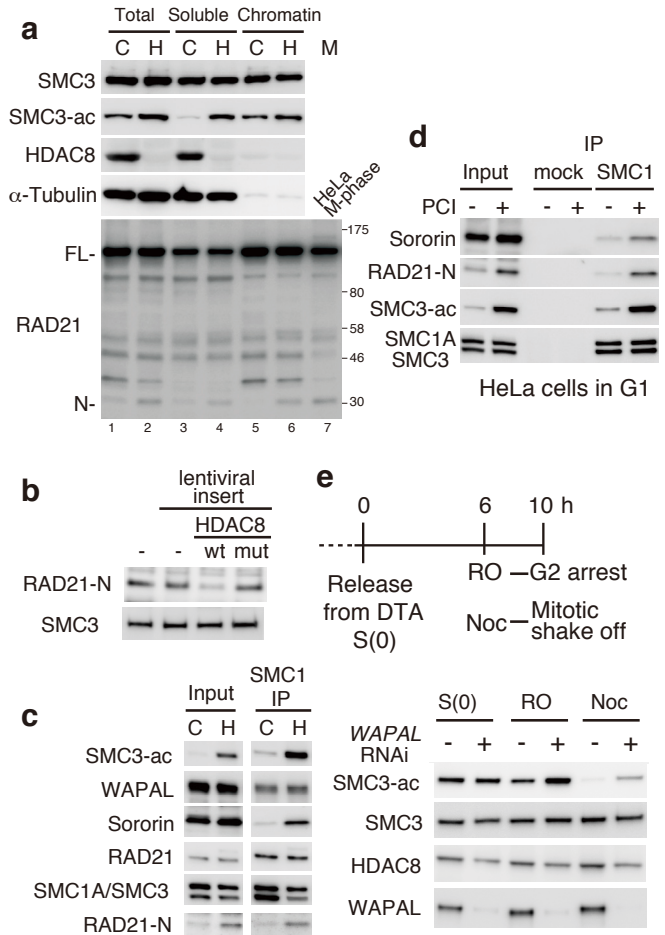
a, Extracts of control (C) and HDAC8-mutant LCLs (H; p.G320R) were fractionated into soluble and chromatin fractions. The soluble fraction extracts from late M phase HeLa cells were prepared and analyzed in lane 7. Immunoblotting of SMC3, SMC3-ac, HDAC8, α -Tubulin and RAD21 were performed. "FL" and "N" indicates full-length and the cleaved N-terminal fragment of RAD21, respectively. Although faintly visible in the soluble fraction in control cells as previously reported¹⁴, the N-terminal fragment is increased with the loss of HDAC8.

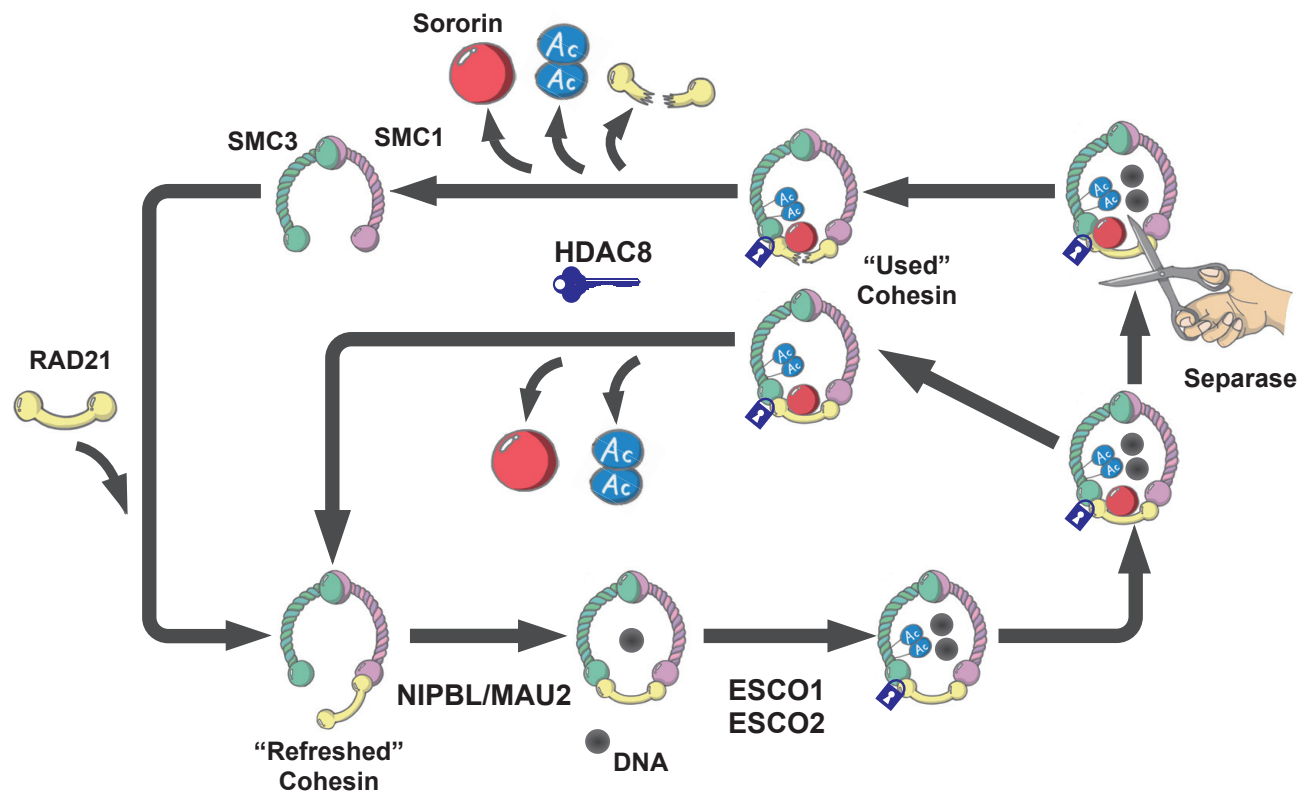
b, The N-terminal fragment of RAD21 (RAD21-N) was detected by immunoblotting with a fragment-specific antibody^{14,15} to be stabilized in the lysates from lentiviral-rescued proband fibroblasts studied in Supplementary Fig. 8.

c, To ascertain if this additional Sororin is complexed to cohesin containing residually acetylated SMC3 bound to RAD21 cleavage products, SMC1A was immunoprecipitated from soluble extracts prepared from normal (C) and HDAC8-mutant (H) LCLs. Immunoblot analysis was performed using the indicated antibodies.

d, Total cell extracts were obtained from synchronized HeLa cells 12 hr after release from double thymidine arrest following progression through mitosis and harvested in G1. Control and SMC1A immunoprecipitations from the extracts were analyzed by immunoblotting using the indicated antibodies.

e, HeLa cells were transfected with WAPAL siRNA and subsequently synchronized in early S phase by double thymidine arrest (S(0)). RO-3306 and nocodazole were added at 6 h from release of synchronization to arrest at the G2/M boundary or in metaphase, respectively. The cells treated with RO were collected at 10 h from release. The cells treated with nocodazole were collected by mitotic shake off at same time point. Total cell extracts were analyzed by immunoblotting using indicated antibodies.





Supplementary Figure 10 | A model for the role of HDAC8.

Cohesin, containing nonacetylated SMC3, is loaded onto chromosomes under the direction of NIPBL and MAU2. Loading of cohesin containing nonacetylated SMC3 is required for cohesion establishment in S phase, when SMC3 is acetylated by ESCO1/ESCO2 to facilitate binding of Sororin. Cohesin is removed by either the prophase pathway or by separase-dependent cleavage of RAD21 at anaphase onset. Upon removal from chromatin, HDAC8 deacetylates SMC3 to facilitate release of RAD21 and Sororin, thereby efficiently “refreshing” cohesin “used” in the previous cell cycle. This allows reacetylation of SMC3 in the following cell cycle to ensure its full functionality in sister chromatid cohesion and transcriptional regulation.

Supplementary Discussion

Conservation of the acetylation-deacetylation cycle

Our data confirm that the acetylation-deacetylation cycle of SMC3 is a conserved mechanism among eukaryotes. Localization of SMC3-ac is restricted on chromosomes in humans, consistent with that previously shown for *S. cerevisiae*¹⁶⁻¹⁸. In yeast, the acetylation of SMC3 dramatically decreases in the *scc2/4* cohesin loader mutant, and has been suggested that cohesin acetylation takes place only on chromosomes by the acetyltransferase, ECO1, a component of the replication machinery¹⁹. In juxtaposition, the yeast deacetylase HOS1 is localized in the soluble fraction and acts on SMC3-ac that is dissociated from chromosomes¹⁶. Likewise, in humans, where there are at least two SMC3 acetyltransferases, ESCO1 and ESCO2, both of which are chromatin-bound (data not shown), while HDAC8 resides in the soluble fraction. Furthermore, cohesion defects observed by double knock down of both HDAC8, which reduces SMC3-deacetylase activity, and SMC3, which reduces new SMC3 production (Supplementary Fig. 4), implies that an increased SMC3-ac:SMC3 ratio interferes with cohesion establishment as shown for yeast. This is also consistent with the requirement for *de novo* acetylation of SMC3 on chromosomes, either directly or indirectly, for establishment of sister chromatid cohesion in humans.

HDAC8 in CdLS and human disease

We have presented cellular, biochemical genetic and genomic data demonstrating a role for human HDAC8 in the deacetylation of SMC3 and subsequent regulation of cohesin in human development. HDACs have been associated with human malignancy²⁰ and HDAC4 has recently been implicated in the Brachydactyly Mental Retardation syndrome (BDMR; OMIM 600430²¹). However, this work is the first to demonstrate a clear and direct mechanism for a lysine deacetylase in a germline human disorder. Furthermore, this data clearly implicates a non-histone protein acetylation target, SMC3, in the pathogenic process and connects HDAC8 and cohesin in human development, as mutations in either cause closely related phenotypes.

Consistent with clinical features described above, a mouse knockout of *HDAC8*²² has demonstrated increased mortality, marked growth abnormalities and defects of dorsal skull development. Of note, the probands identified with *HDAC8* mutations demonstrate small stature, like other probands with CdLS, but this subgroup is notable for large anterior and posterior fontanelles. This is consistent with the mouse model, and may serve as a clinical feature to differentiate this subgroup representing approximately 5% of individuals with CdLS.

While we have presented a clear mechanistic mechanism implicating SMC3-ac as a major functional target of HDAC8 and cohesin recycling in CdLS, we have not formally excluded other proteins as targets of HDAC8, either in the regulation of cohesin or in the pathogenesis of CdLS, and will clearly need to be the focus of future work.

SMC3 deacetylation is necessary to allow dissolution of cohesin establishment interactions and refresh cohesin for maximal function in subsequent cell cycles.

Several CdLS proband cell lines with minimal levels of HDAC8 activity offered us the opportunity to study HDAC8 function directly in human cells with an endogenous mutation. This led to the recognition that loss of HDAC8 activity causes stabilized binding of the separase-cleaved form of RAD21 to cohesin (Fig. 4). It is known that two distinct pathways exist for cohesin removal from chromatin, one to remove cohesin from chromosome arms during prophase and a second to remove it from centromeres in anaphase¹⁴, the latter which involves separase cleavage of RAD21. Our data now clarifies that cohesin removal during the anaphase pathway consists of two steps (Supplementary Fig. 10). The first step is cleavage of RAD21 by separase. However, the removal of RAD21 cleavage fragments and Sororin requires a second step, deacetylation of SMC3, for their efficient release. It is clear that the SMC3-ac containing cohesin complex has a higher affinity for the RAD21 N- and C-terminal fragments as well as for Sororin, but it is not yet clear whether this binding is via direct interaction of one of these components with the acetylated residues of SMC3 or by other alterations may result from this acetylation.

Nonetheless, these findings are consistent with acetylation acting as a “lock” for the cohesin ring by stabilizing the interaction between RAD21, SMC3 and Sororin to facilitate establishment of sister-chromatid cohesion during replication. The HDAC8-coordinated release of SMC3 from this “locked” mode by deacetylation appears to be essential for the removal of Sororin and cleaved RAD21. Our data does not suggest that HDAC8 is necessary for cohesin release from chromatin. It however, appears to act upon released acetylated cohesin to allow it to be recycled and fully functional in the following cell cycle. We also see evidence in ChIP-Seq data (Figs. 2a-c and Supplementary Figs. 5e-h, 7a,b and 8b,c), as well from cell synchronization experiments (Figs. 1d,e, 4d-g and Supplementary Fig 9a) that acetylated cohesin may be able to be reloaded, but based on our ChIP-Seq data, it has reduced presence at its normal localization sites, due either to decreased loading or stability on chromatin.

This is quite relevant in the context of CdLS, which in its classic form, is typically caused by mutations in the cohesin loader *NIPBL*. The clinical similarity of children with *HDAC8* and *NIPBL* mutations demonstrate a clear phenotypic similarity that is paralleled by ChIP-Seq data. This demonstrates decreased amounts of cohesin at localization sites on chromatin with in the setting of reduced HDAC8 activity, a finding previously observed for CdLS caused by *NIPBL* haploinsufficiency.

In summary, we have noted that HDAC8 functions as a human SMC3 deacetylase. While loss of HDAC8 does not markedly alter the removal of cohesin from chromatin, HDAC8 appears to be required for the deacetylation of “used” cohesin to recycle it for subsequent cell cycles. We have noted mutations in *HDAC8* cause features of “classical” CdLS, also caused by mutations in *NIPBL*. We propose a common mechanism, whereby loss of either HDAC8 or *NIPBL* to result in normally localized cohesin, but decreased occupancy of localization sites. In the case of *NIPBL*, this likely arises from defective loading, while in the case of HDAC8, from either improperly loaded or reduced stability of SMC3 containing residual acetylation on chromatin.

It is clear that further work in cellular and developmental models will be crucial to elucidating the mechanisms by which mutations in these molecules alter cohesin function and to result in the specific transcriptional dysregulation that result in the clinically unique features recognized in CdLS.

SUPPLEMENTARY TABLES

Supplementary Table 1. Clinical features of individuals with HDAC8 mutations.

Mutation	Protein Effect	Clinical features
c.490C>T	nonsense p.R164X	CDLG13952; <i>de novo</i> mutation; 6y heterozygous female with growth delays, absent speech and facial features consistent with CdLS. Asymmetric skull, limb length discrepancy, dysplastic kidneys.
c.539A>G	missense p.H180R	CDL016P; <i>de novo</i> mutation; heterozygous female seen at 3y died in teens. Growth and facial features consistent with severe CdLS. Moderate to severe cognitive impairment, no limb anomalies.
c.932C>T	missense p.T311M	CDL279P; <i>de novo</i> mutation; 1y heterozygous female with severe growth and cognitive delays and facial features of classic CdLS. Large skull fontanelles, pulmonary stenosis and unilateral hearing loss. No limb deficiency.
c.958G>A	missense p.G320R	CDL426P; <i>de novo</i> mutation; 5y hemizygous male with severe cognitive and growth delays and facial features consistent with CdLS. Large skull fontanelles, atrial septum aneurysm, bilateral hearing loss, happy personality noted.
c.1001A>G	missense p.H334R	CDL248P; <i>de novo</i> mutation; 7y heterozygous female with severe cognitive and growth delays and facial features suggestive of CdLS. Delayed fontanelle closure, limb length difference but no deficiencies, happy and introverted. Family CDL326; familial mutation; 13y hemizygous male proband with severe cognitive and growth delay and facial features suggestive of CdLS. 8y mildly heterozygous affected sister with mild cognitive and growth delays and mildly overlapping facial features. Unaffected heterozygous mother.
CdLS, Cornelia de Lange Syndrome		

Supplementary Table 2. siRNA sequences used in this study

NAME	SENSE	ANTISENSE
HDAC1-1	GCCUGUGAGGAAGAGUUCUCCGAUU	AAUCGGAGAACUCUCCUCACAGGC
HDAC1-2	UGGCCAUCCUGGAACUGCUAAAAGUA	UACUUUAGCAGUUCAGGAUGGCCA
HDAC2-1	UCUAACAGUCAAAAGUCAUGCUGAAA	UUUAGCAUGACCUUUGACUGUUAGA
HDAC2-2	GAAGAUCCAGACAAGAGAAUUUCUA	UAGAAAUUCUCUUGUCUGGAUCUUC
HDAC3-1	CCAUGCCAAGAAGUUUGAGGCCUCU	AGAGGCCUCAACUUCUUGGCAUGG
HDAC3-2	CGGGAUGGCAUUGAUGACCAGAGUU	AACUCUGGCAUCAAAUGCCAUCCCG
HDAC4-1	CCACCGGAAUCUGAACCACUGCAUU	AAUGCAGUGGUUCAGAUUCCGGUGG
HDAC4-2	UCGUGUAUGACACGCUGAUGCUGAA	UUCAGCAUCAGCGUGUCAUACACGA
HDAC5-1	CAGAAACAGCAUGACCACCUGACAA	UUGUCAGGUGGUCAUGCUGUUUCUG
HDAC5-2	CAAGUUAUGAGCACAUCCUCUAUU	AAUAGAGGAUGUGCUGAUAACUUG
HDAC6-1	CCAGCACAGUCUUAUGGAUGGCUAU	AUAGCCAUCCAUAAGACUGUGCUGG
HDAC6-2	AGUUCCAACUUUGACUCCAUCUAUA	UAUAGAUGGAGUCAAAAGUUGAACU
HDAC7-1	GCACCCUCAGGUGUUGCUCUGGGAA	UUCCCAGAGCAACACCUGAGGGUGC
HDAC7-2	GAGCCCAUGAGGCUCUCCAUGGACA	UGUCCAUGGAGAGCCUCAUGGGCUC
HDAC8-1	GGCCACCUUCCACACUGAUGCUGAU	AUAAGCAUCAGUGUGGAAGGUGGCC
HDAC8-2	GACGGAAAUUUGAGCGUAUUCUCUA	UAGAGAAUACGCUCAAAUUCGGUC
HDAC9-1	CCUACUGAGUAAAUCAGCAACGAAA	UUUCGUUGCUGAUUUACUCAGUAGG
HDAC9-2	GAACAAACUGCUUUCGAAUUCUAUU	AAUAGAUUUCGAAAGCAGUUUGUUC
HDAC10-1	CGGAGUCAGUGUGCAUGACAGUACA	UGUACUGUCAUGCACACUGACUCCG
HDAC10-2	UCACUGCACUUGGGAAGCUCCUGUA	UACAGGAGCUUCCCAAGUGCAGUGA
HDAC11-1	UCUCCAGGGCUACCAUCAUUGAUCU	AGAUCAAUGAUGGUAGCCCUGGAGA
HDAC11-2	GACGUGGUGGUUAUACAAUGCAGGCA	UGCCUGCAUUGUAUACCACCACGUC
SIRT1-1	CCCAUGAAGUGCCUCAGAUUUAAU	AUUAAUAUCUGAGGCACUUAUGGG
SIRT1-2	CCAAACUUUGCUGUAACCCUGUAAA	UUUACAGGGUUACAGCAAAGUUUGG
SIRT2-1	ACAUGGACUCCUGCGGAACUUUU	AAUAAGUUCGCGAGGAAGUCCAUGU
SIRT2-2	GAGGCCAUCUUUGAGAUACAGCUAUU	AAUAGCUGAUCUCAAGAUUGGCCUC
SIRT3-1	CCUGCAGGAUGUAGCUGAGCUGAUU	AAUCAGCUCAGCUACAUCUGCAGG
SIRT3-2	GCUGGUUGAAGCUAUGGAACCUUU	AAAGGUUCCAUGAGCUUCAACCAGC
SIRT4-1	GAGAAACUUCGUAGGCUGGCCUCAA	UUGAGGCCAGCCUACGAAGUUUCUC
SIRT4-2	GCUGUGGAAGCUAUUCGAUUGGUUA	UUCAGAUGGCCUCCACAUUGAACGC
SIRT5-1	CCAAGUCGAUUGAUUCCAGCUAU	AUAGCUGGGAAAUCAAUCGACUUGG
SIRT5-2	CCAGCGUCCACACGAAACCAGAUUU	AAAUCUGGUUUCGUGUGGACGCUGG
SIRT6-1	GCUUCCUGGUCAGCCAGAACGUGGA	UCCACGUUCUGGCUGACCAGGAAGC
SIRT6-2	CAUCGUCAACCUGCAGCCACCAAG	CUUGGUGGGCUGCAGGUUGACGAUG
SIRT7-1	CCAACAGGGAGUACGUGCGGGUGUU	AACACCCGCACGUACUCCUGUUGG
SIRT7-2	GCCAGCAGAGCAGACACCAUCCUGU	ACAGGAUGGUGUCUGCUCUGCUGGC
SMC3	GGAGGGCAGUCAGUCUCAAGAUGAA	UUCAUCUUGAGACUGACUGCCCUCC
HDAC8	UCAACUACAUCAAAGGGAAUCUGAA	UUCAGAUUCCCUUUGAUGUAGUUGA
WAPAL	CCCUUACUUCUAAACGAGCAGGAGA	UCUCCUGCUGUUUAGAAGUAAGGG

Supplementary Table 3. CdLS lymphoblastoid expression profile genes.

Gene	Accession	Targeted Region	Nanostring Target Sequence	Use
ADCY1	NM_021116.2	12105-12205	GAATGGAGAGTGATGTGGGCAAGGGTGTCTATTTCTCGCACATAACAACCTCACTGAGGATGCTTCTGTAGAAGTGAGAAACACGATGAGTACATTCAGAA	CdLS expression profiling
AI250445	AI250445.1	1-101	GACCAATTGGTGCCTCGCAGCCACGCTGGGGCTTCTTTATCTCAGGGGCAGGAACACATAAAAGGCTTATTTACAAGACGAACCCGCGGCTGCAGGC	CdLS expression profiling
AI770171	AI770171.1	376-476	TCCATTCAAAGCTGAACCTCAGCAGCGAGGATTTATTTCTGGTCAGCCAACAGCTGCATAAAGGTAGAATGTTAATAACCCCTTCACTTCCAGCTCCAGGAC	CdLS expression profiling
AIM1	NM_001624.2	7093-7193	TTTCAAAATGCAAAACAACTGCTTTAAACACTGACAAGACACCCAGCCCATACGCTGCTCTTCCAACAGTGGGTTCTAGCTTTGAACAAAAGTGCTAAACAT	CdLS expression profiling
ARHGAP24	NM_001025616.2	2620-2720	GTTTTTTTCCACGTTTGAGAACTGACAGTGAACCCAGGAGAACCAGAGAGAGGAAACACAATATGGATTCACTGAGCCTGCTTTCCGCTGCTGTCTCTG	CdLS expression profiling
ARL8A	NM_138795.2	1256-1356	GCAGGTACCAGCCTGGGCACTGGTGCCGCGCTCCCTGTCCCGTGTGTTCCACCGCCCAATCTGGCTTGCTTGGCAGTGCTTGAATGCCACAGGCTGGC	CdLS expression profiling
ATP10D	NM_020453.3	5498-5598	TGAGGACAGGAATGCTATAGCAAGTTTACTCCTATTGCGAATCATGTATGCTGGCTTTAGTTGTAACAAACGATTTTATTCTAAGTAAGGCCAGGTGCT	CdLS expression profiling
AW500340	AW500340.1	55-155	GTGTGCTCCAACCACCAACCTTTCAACATTTAACTGAATGAATGAATATAACCTCTTCAAGGTTCACTGTTTTCATAAGCAAAACAGAGAATAGCAGC	CdLS expression profiling
CXXC1	NM_001101654.1	2759-2859	GAGCCGCCCGGTGCCCGTGTGCCGTTCTCCACTCATCTGTTTCTCCGGTTCTCCCTGTGCCCATCCACCGGTTGACCGCCCATCTGCCTTTATCAGAG	CdLS expression profiling
FGD6	NM_018351.3	4545-4645	CCAAGAGGTGGAATTTTCATCAGAATGGAGTAAATGCAATTCAAAAATGTATAAAAAATGAACACTGCCAAGATAAAGCCAAACAGACCCCTTCATCAAAAG	CdLS expression profiling
FNIP2	NM_020840.1	5437-5537	TGGCAGTTCATAATTAGACCCATATAGGGGACACTGAGCTTTAACTCGTTGATTTCTAAACTCTATACATATAAAAAAATTACGCCAGGCCCCCTCAAAAGC	CdLS expression profiling
GLOXD1	NM_032756.2	1197-1297	GCTCCAGCAGGGATCCTGCTAGATGGTGATAAAGCAAGTTTCTGCTTCAGTCTTCCACCAAGTCCCTTTTCACTGAGGACACTTTCTTCTGGAGCTGA	CdLS expression profiling
ID3	NM_002167.3	688-788	CCACACTTCCCATCCAGACCGCAGCTGATCCTCGGAAGTTGCTATCTCCAACGACAAAAGAGCTTTTGCCACTGACTCGGCCGTGCTGCTGACACCTCC	CdLS expression profiling
JDP2	NM_130469.3	1665-1765	GGCGGGGTGCATTTCCATCCTGTAAACCCCTCATAGTACTCAGTCTGTATCGCTCAGTAAACATTGCTCTTACTTACATAGCCGCCTTGCCTGGTGTCT	CdLS expression profiling
KIFAP3	NM_014970.2	2275-2375	AAGAAAAATTCAGAGTGAAAAGTTTCGCTGGCATAACTCTCAGTGGCTGGAGATGGTAGAGAGTCGTAGATGGATGAGAGTGAGCAGTACTTGTATGGTG	CdLS expression profiling
LTB	NM_002341.1	330-430	AGGAACAGGCGTTTCTGACGAGCGGGACGCAGTCTCGGACGCCGAGGGGCTGGCGCTCCCGCAGGACGGCTCTATTACCTCTACTGTCTCGTCGGCTA	CdLS expression profiling
NIPBL	NM_015384.4	8553-8653	GCGGAGGAGGAGTCAACGTATTTCCGACGCTATTACGTAATGATTTTTATGTGCTTATATATGTCAGTCTATTAATGTACACCAAGTAATGTAATAC	CdLS expression profiling
NMB	NM_021077.3	761-861	CTGGTACAATACTCGAGAAATGACACCAATAATGGGCGAGACACAACAGCGTGGCTTAGATTGTGCCACCCAGGGAAGGTGCTGAATGGGACCCCTGTT	CdLS expression profiling
PAPSS2	NM_004670.3	3210-3310	ATTCCTCTCAGCTGCTTAACAAAGTTCCTCGAACAGAAAGTGCTTACAAAGCTGCCTTCTCGGATACTGAAAGGTCGAGTTTTCTGAACTGCACTGATTT	CdLS expression profiling
PCDHGC5	NM_018929.2	4069-4169	CTTCAACAGGGCCCCCTGCCCTCTGAAGCCTCAGTCCCTCACCTTGCCAGGTGCCGTTTCTCTCCGTGAAGGCCACTGCCAGGTCCCCAGTGCCGCCCC	CdLS expression profiling
PHF16	NM_014735.3	4563-4663	GTAGCCTTTGTCCCTTCATGCTTTCAATTCTGAGTGGGAGGAAAGCAACATCAAAACAGTGCTTCAGCCAAATTCATATGTAATGCCATTGGGAGA	CdLS expression profiling
PRR6	NM_181716.2	605-705	TTCAATTGTTCCAGCTTCTCGCTTCAAGCTCCTGAAGGAGCTGAGCACAATACGACTATACAGTTCAACTATCAACAAAGCCAGCATACCTTCTGTAAGA	CdLS expression profiling
PTHB1	NM_014451.3	3164-3264	CTCACCTTCTGGAGATGACATCAGATAGAACGAGGGGTTGGGACTTTTTACTTCACTAGGAGAACTGTAAACACCATGGGAGTCAAGTGAACTTTGTCT	CdLS expression profiling
PTPN18	NM_014369.3	3420-3520	CCTCTGTGTTGCTGGATAATGAGTCATCTATCTCTGGAGGAGAAGAAAGGCAGGTCTCCACAGCCCTGATAAAATCTCCAAGTCTCCGAGTTTCGGGTC	CdLS expression profiling
RHOBTB3	NM_014899.3	2512-2612	TCCTTGAAAAAAACTACCACTGTGGTCTTAAAGGGAACAAAATATACCATAGGCTAAAACTAAGGCTTTCACTCTAGAATGCAAAGCTGTTTGCAGC	CdLS expression profiling
ROBO1	NM_002941.2	6395-6495	TGAACCACAAAAAAAGGCTGGTGTTACCAAAACCAAACTTGTTCAATTTAGATAATTTGAAAAAGTTCCATAGAAAAGGCGTGCACTACTAAGGGAAC	CdLS expression profiling
SLC6A6	NM_003043.3	3956-4056	AAGGGCAATTCTGAACCCCATCTTTGGCAGGCATACATATTTCACTGTTTCCAAAGCTATCTACTCTGCCAAACACACCCAGTCTCTATTTCCAAACTCT	CdLS expression profiling
SNX30	NM_001012994.1	7175-7275	GTCCACCGTGATAATGTTACCTTCTCTCATGCTGCCATTATGCCAAAACAAAAGCTGTGATAAAAAAGTGCTTGAGAGAGTGTTGATAAGAAAAGTG	CdLS expression profiling
TRERF1	NM_033502.2	6904-7004	TCAGGTTTGCACTATTATAAGTTGACATCATAATATCTAGTGTGCTTAACTGTATTTTCCCGAATGCAAGTCCCTTGGTCCATATTAAGCACTATGTA	CdLS expression profiling
TSPAN12	NM_012338.3	2087-2187	TACCAGTGTGATACATAGGAATCATTATTCAGAATGTAGTCTGGTCTTTAGGAAGTATTAATAAGAAAAATTTGCACATAAATTAGTTGATTGAGAAAAGGA	CdLS expression profiling
ZNF608	NM_020747.2	5262-5362	ACTTTTGAAGGCAATGGGGTTGCCAGTAGCCAAAAAACTGTGTTGATATAATGTAAGATTAAATGGGAAATTAATGAGCACTGTGAATATGAGGT	CdLS expression profiling
ZNF695	NM_020394.3	1195-1295	ACCTTCCGATGTGAAGAATGTGGAAGAGCCCTTAACACAGAGCTCACATCTGACTGAACATAGGAGAATTACTGGTGAGAACCATCAAAATGTGAGG	CdLS expression profiling
ACTB	NM_001101.2	1010-1110	TGCAGAAGGAGATCACTGCCCTGGCAGCCAGCAATGAAGATCAAGATCACTTGCTCTCTCTGAGCGCAAGTACTCCGTGTGGATCGCGGCTCCATCTCT	Normalization
RPL19	NM_000981.3	315-415	CCAATGCCCGAATGCCAGAGAAGGTACATGGATGAGGAGAATGAGGATTTTGCGCCGGCTGCTCAGAAGATACCGTGAATCTAAGAAGATCGATCGCCA	Normalization

Supplementary Table 4. Primers used for ChIP-qPCR.

Primer ID	Left Primer	Right Primer	Chromosome position (hg19)
NH1	GCTCTGCTGACTGGCACC	CTCACCTTGAAGGAGCAATAAG	chr9:128,979,088-128,979,307
NH2	ACATGCCTGATGCACATGAC	AGTCAATGAGTGCCATGCTC	chr13:29,583,060-29,583,274
NB1	AGCACAGGCAATGGTGTTAG	TTGAATGGAGCACTGTGGAG	chr2:118,308,132-118,308,329
NB2	CACTTCCAACCACACGAGG	TCAGGACGTCTTACCTGAGTAGG	chr13:112,737,44-112,737,664
PH1	GCAAGGCTCTACCGTCATTC	CCTTCTCTTCAGAAAGCCGTG	chr12:38,787,634-38,787,825
PH2/PB1	GGCAGTTCCAGCACATCC	GAATGGCGACACCGAAC	chr15:41,983,359-41,983,571
PH3/PB2	GTGATCGGTCCAGTGCATAG	CTGGCATGTCTATGGTAGAGC	chr1:55,716-55,937
PH4	GTTCAACTGGTACTGCTGCC	TGGTTCTAGGCAATTGGTAAGTC	chr2:118,477,171-118,477,382
PB3	TGAAGCCACCACCTGCTTAG	TCTTGCATGTGAGCGAGAAC	chr21:34,218,281-34,218,465
PB4	ATGGCAACACTGCTCTTCAG	TAGAGCACAGCCATAGGTGG	chr5:131,750,332-131,750,553
PB5	CAGCTTGTCTGCTGCTTAGC	TGACCATCGGCAAGAAGG	chr6:41,678,731-41,678,954
PH5/PB6	TGTACACCTCACGGAAGCAG	AAGCAGGCAACAGGCAAC	chr6:73,896,272-73,896,470

Supplementary Table 5. ChIP and RNA sequencing and mapping statistics

ChIP-seq						
Cells	Sample description RNAi, IP, replicate	Platform	Mapping tool (param)	Reference	Reads	Mapped
HeLa	CON, SMC3ac, #1	SOLiD5500	Bowtie-0.12.5 (-n3 -m1)	UCSC hg19	121,365,117	76858901 (63.33%)
	CON, SMC3ac, #2	SOLiD5500	Bowtie-0.12.5 (-n3 -m1)	UCSC hg19	63,279,518	39757011 (62.83%)
	HDAC8, SMC3ac, #1	SOLiD5500	Bowtie-0.12.5 (-n3 -m1)	UCSC hg19	106,276,377	68273036 (64.24%)
	HDAC8, SMC3ac, #2	SOLiD5500	Bowtie-0.12.5 (-n3 -m1)	UCSC hg19	57,881,700	36815899 (63.61%)
	CON, RAD21, #1	SOLiD5500	Bowtie-0.12.5 (-n3 -m1)	UCSC hg19	76,354,774	49710310 (65.10%)
	CON, RAD21, #2	SOLiD5500	Bowtie-0.12.5 (-n3 -m1)	UCSC hg19	46,320,711	29698509 (64.11%)
	HDAC8, RAD21, #1	SOLiD5500	Bowtie-0.12.5 (-n3 -m1)	UCSC hg19	70,262,088	45487413 (64.74%)
	HDAC8, RAD21, #1	SOLiD5500	Bowtie-0.12.5 (-n3 -m1)	UCSC hg19	59,172,203	37469237 (63.32%)
	CON input	SOLiD5500	Bowtie-0.12.5 (-n3 -m1)	UCSC hg19	111,252,274	67340524 (60.53%)
	HDAC8 input	SOLiD5500	Bowtie-0.12.5 (-n3 -m1)	UCSC hg19	104,057,244	67492200 (64.86%)
	CON, CTCF, #1	SOLiD5500	Bowtie-0.12.5 (-n3 -m1)	UCSC hg19	42,742,350	28754821 (67.27%)
	CON, CTCF, #2	SOLiD5500	Bowtie-0.12.5 (-n3 -m1)	UCSC hg19	50,299,149	33945452 (67.49%)
	CON, CTCF input	SOLiD5500	Bowtie-0.12.5 (-n3 -m1)	UCSC hg19	57,679,610	38696452 (67.09%)
Fibroblasts	WT, SMC3ac	SOLiD5500	Bowtie-0.12.5 (-n3 -m1)	UCSC hg19	68,093,188	44802597 (65.80%)
	Mut, SMC3ac	SOLiD5500	Bowtie-0.12.5 (-n3 -m1)	UCSC hg19	68,862,351	45270523 (65.74%)
	WT, RAD21	SOLiD5500	Bowtie-0.12.5 (-n3 -m1)	UCSC hg19	65,655,576	38110914 (58.05%)
	Mut, RAD21	SOLiD5500	Bowtie-0.12.5 (-n3 -m1)	UCSC hg19	50,510,641	29212173 (57.83%)
	WT input	SOLiD5500	Bowtie-0.12.5 (-n3 -m1)	UCSC hg19	63,513,838	44394023 (69.90%)
	Mut input	SOLiD5500	Bowtie-0.12.5 (-n3 -m1)	UCSC hg19	73,516,535	50888948 (69.22%)
LCLs	CON, SMC3ac	SOLiD3	Bowtie-0.12.5 (-n3 -m1)	UCSC hg19	72,522,819	39557704 (54.55%)
	HDAC8, SMC3ac	SOLiD3	Bowtie-0.12.5 (-n3 -m1)	UCSC hg19	75,034,284	44078954 (58.75%)
	CON, RAD21	SOLiD3	Bowtie-0.12.5 (-n3 -m1)	UCSC hg19	69,875,098	41353001 (59.18%)
	HDAC8, RAD21	SOLiD3	Bowtie-0.12.5 (-n3 -m1)	UCSC hg19	52,577,685	31607471 (60.12%)
	CON input	SOLiD3	Bowtie-0.12.5 (-n3 -m1)	UCSC hg19	54,896,723	34818443 (63.43%)
	HDAC8 input	SOLiD3	Bowtie-0.12.5 (-n3 -m1)	UCSC hg19	60,284,140	37432087 (62.09%)
RNA-seq						
Cells	Sample description	Platform	Mapping tool (param)	Reference	Reads	Mapped
Fibroblasts	WT, #1	Hiseq	Bowtie-0.12.5 (-n3 -m10 -a)	Refseq mRNA (NM*)	65,018,037	53909114 (82.91%)
	WT, #2	Hiseq	Bowtie-0.12.5 (-n3 -m10 -a)	Refseq mRNA (NM*)	59,441,894	48431555 (81.48%)
	Mut, #1	Hiseq	Bowtie-0.12.5 (-n3 -m10 -a)	Refseq mRNA (NM*)	48,190,251	39839903 (82.67%)
	Mut, #2	Hiseq	Bowtie-0.12.5 (-n3 -m10 -a)	Refseq mRNA (NM*)	49,016,399	40290754 (82.20%)

Supplementary Table 6. Peak calling summary statistics.

cells	antibody	sample	peak number	FDR(%)	total peaks width (bp)	FDR(%)
HeLa Rep 1	RAD21	CON	32,263	0.29	47,497,417	0.15
		HDAC8	27,146	0.36	39,456,544	0.18
	SMC3ac	CON	4,673	0.11	5,596,067	0.06
		HDAC8	4,270	0.09	4,580,800	0.07
	CTCF	WT	53,135	0.36	91,434,535	0.16
HeLa Rep 2	RAD21	CON	33,530	0.34	49,146,580	0.19
		HDAC8	27,229	0.38	39,392,001	0.20
	SMC3ac	CON	5,220	0.13	6,129,770	0.09
		HDAC8	4,702	0.34	5,028,008	0.20
	CTCF	CON	54,519	0.37	95,289,111	0.16
HeLa Common	RAD21	CON	29,671	n/a	45,112,339	n/a
		HDAC8	24,614	n/a	37,120,426	n/a
	SMC3ac	CON	3,769	n/a	4,788,411	n/a
		HDAC8	3,167	n/a	3,622,793	n/a
	CTCF	CON	50,518	n/a	89,092,312	n/a
Fibroblasts	RAD21	WT	42,019	0.15	67,901,781	0.07
		Mut	35,120	0.07	52,423,060	0.03
	SMC3ac	WT	517	1.93	374,393	1.94
		Mut	1,443	0.28	1,399,727	0.30
LCLs	RAD21	CON	25,780	0.06	47,083,170	0.04
		HDAC8	19,056	0.06	30,580,644	0.03
	SMC3ac	CON	517	1.93	456,453	1.54
		HDAC8	5,647	0.09	6,354,753	0.09

Supplementary Table 7.

Genes expressed in fibroblasts detected by RNA Sequencing (Microsoft Excel file).

Supplementary Table 8. Genes upregulated 1.2-fold or greater in skin fibroblasts expressing mutant HDAC8 vs. wild type HDAC8. (n=56)

Gene Name	Description	Gene Length	WT Rep 1	WT Rep 2	Mut Rep 1	Mut Rep 2	Mut/ WT
ITGA7	integrin, alpha 7 (ITGA7)	4150	4.33	4.6	7.59	6.39	1.57
RDH5	retinol dehydrogenase 5 (11-cis/9-cis) (RDH5)	1359	3.73	3.7	5.75	4.88	1.43
TEK	TEK tyrosine kinase, endothelial (TEK)	4817	5.3	4.77	6.9	7.22	1.4
C11orf96	chromosome 11 open reading frame 96 (C11orf96)	1361	2.57	2.73	3.99	3.37	1.39
PI16	peptidase inhibitor 16 (PI16)	2205	9.8	10.24	14.6	13.05	1.38
AK4	adenylate kinase 4 (AK4), nuclear gene encoding mitochondrial protein	6998	3.55	3.71	4.82	5.02	1.36
TRNP1	TMF1-regulated nuclear protein 1 (TRNP1)	1949	30.97	32.48	44.23	41.91	1.36
C4orf31	chromosome 4 open reading frame 31 (C4orf31)	2911	16.11	15.39	20.74	22.14	1.36
COMP	cartilage oligomeric matrix protein (COMP)	2471	8.12	8.56	12.03	10.53	1.35
C4orf48	chromosome 4 open reading frame 48 (C4orf48)	483	9.46	17.52	20.57	15.72	1.35
C3	complement component 3 (C3)	5101	4.47	4.56	6.32	5.75	1.34
C11orf1	chromosome 11 open reading frame 1 (C11orf1)	984	2.78	2.44	3.16	3.78	1.33
NES	nestin (NES)	5591	10.57	11.67	14.94	14.47	1.32
B9D1	B9 protein domain 1 (B9D1)	932	4.04	4.9	6.4	5.31	1.31
CNTN3	contactin 3 (plasmacytoma associated) (CNTN3)	4997	2.72	2.59	3.33	3.56	1.3
ODZ2	odz, odd Oz/ten-m homolog 2 (Drosophila) (ODZ2)	9645	21.04	20.29	27.41	25.91	1.29
IFIT1	interferon-induced protein with tetratricopeptide repeats 1 (IFIT1)	1876	3.84	4.04	4.72	5.41	1.29
PYGL	phosphorylase, glycogen, liver (PYGL)	2859	10.5	10.19	12.83	13.55	1.28
PODXL	podocalyxin-like (PODXL)	6007	230.25	234.86	299.08	294.61	1.28
AOX1	aldehyde oxidase 1 (AOX1)	4949	8.88	9.27	11.31	11.76	1.27
CCL26	chemokine (C-C motif) ligand 26 (CCL26)	562	5.91	4.95	7.37	6.39	1.27
CPA4	carboxypeptidase A4 (CPA4)	2817	4.65	5.09	6.16	6.23	1.27
FAM24B	family with sequence similarity 24, member B (FAM24B)	788	3.72	4.64	5.58	4.94	1.26
GP6R	G protein-coupled estrogen receptor 1 (GP6R)	2981	3.73	3.88	5.14	4.37	1.25
KIT	v-kit Hardy-Zuckerman 4 feline sarcoma viral oncogene homolog (KIT)	5190	3.06	2.83	3.56	3.8	1.25
KIAA1217	KIAA1217 (KIAA1217)	7773	3.93	3.66	4.62	4.89	1.25
NETO2	neuropilin (NRP) and tolloid (TLL)-like 2 (NETO2)	3692	2.64	2.62	3.25	3.3	1.25
MATN2	matrilin 2 (MATN2)	4122	27.95	28.71	35.28	34.79	1.24
ANKRD9	ankyrin repeat domain 9 (ANKRD9)	1626	6.27	8.98	10.66	8.2	1.24
XRCC6BP1	XRCC6 binding protein 1 (XRCC6BP1)	1182	3.61	3.17	4.18	4.2	1.24
RNF182	ring finger protein 182 (RNF182)	3505	4.64	4.62	5.61	5.87	1.24
ST6GALNAC5	ST6 (alpha-N-acetyl-neuraminy-2,3-beta-galactosyl-1,3)-N-acetylglucosaminide alpha-2,6-sialyltransferase 5 (ST6GALNAC5)	2048	4.07	4.1	5.12	5.01	1.24
MEIR5	MEI5 meiotic recombination protein homolog (S. cerevisiae) (MEIR5)	1518	4.42	4.66	4.82	6.32	1.23
CCNG2	cyclin G2 (CCNG2)	5489	6.35	6.51	7.59	8.17	1.23
SEMA4B	sema domain, immunoglobulin domain (Ig), transmembrane domain (TM) and short cytoplasmic domain, (semaphorin) 4B (SEMA4B)	3814	2.75	2.64	3.44	3.2	1.23
PPP1R3C	protein phosphatase 1, regulatory (inhibitor) subunit 3C (PPP1R3C)	2646	28.7	28.86	35.32	35.34	1.23
TSPAN13	tetraspanin 13 (TSPAN13)	1912	26.74	27.32	32.45	34.21	1.23
C2orf74	chromosome 2 open reading frame 74 (C2orf74)	887	3.74	3.74	4.2	5	1.23
LNK1	ligand of numb-protein X 1 (LNK1)	3170	3.06	3.22	3.76	3.91	1.22
ADAMTSL1	ADAMTS-like 1 (ADAMTSL1)	7818	26.67	26.85	33.99	31.07	1.22
ABLIM1	actin binding LIM protein 1 (ABLIM1)	7704	7.57	7.53	9.11	9.27	1.22
TMEM160	transmembrane protein 160 (TMEM160)	696	6.54	12.63	12.26	11.2	1.22
NEURL1B	neuralized homolog 1B (Drosophila) (NEURL1B)	6417	4.88	5.2	6.4	5.78	1.21
SLC35F2	solute carrier family 35, member F2 (SLC35F2)	3184	5.84	5.48	6.76	6.94	1.21
CD9	CD9 molecule (CD9)	1321	17.04	17.41	20.83	20.77	1.21
POLB	polymerase (DNA directed), beta (POLB)	1259	6.17	5.88	7.02	7.55	1.21
NUP35	nucleoporin 35kDa (NUP35)	1649	6.02	6.31	7.31	7.58	1.21
TRIM5	tripartite motif containing 5 (TRIM5)	3659	4.06	3.79	4.78	4.75	1.21
NAP1L3	nucleosome assembly protein 1-like 3 (NAP1L3)	2761	2.92	3	3.44	3.67	1.2
SLC16A4	solute carrier family 16, member 4 (monocarboxylic acid transporter 5) (SLC16A4)	2629	3.35	3.23	3.64	4.25	1.2
TP53INP1	tumor protein p53 inducible nuclear protein 1 (TP53INP1)	5666	3.92	3.87	4.24	5.12	1.2
KLF2	Kruppel-like factor 2 (lung) (KLF2)	1655	13.19	15.38	18.43	15.82	1.2
KIRREL3	kin of IRRE like 3 (Drosophila) (KIRREL3)	3794	9.13	9.66	12.09	10.55	1.2
CFH	complement factor H (CFH)	4200	4.76	4.41	5.32	5.7	1.2
PIK3IP1	phosphoinositide-3-kinase interacting protein 1 (PIK3IP1)	2478	2.49	2.75	3.09	3.22	1.2
CTSC	cathepsin C (CTSC)	6143	9.55	9.12	11.21	11.25	1.2

Supplementary Table 9. Genes downregulated 0.83-fold or less in skin fibroblasts expressing mutant HDAC8 vs. wild type HDAC8. (n=130)

Gene Name	Description	Gene Length	WT Rep 1	WT Rep 2	Mut Rep 1	Mut Rep 2	Mut/ WT
STC1	stanniocalcin 1 (STC1)	3897	7.99	7.28	3.11	3.17	0.41
IL11	interleukin 11 (IL11)	2354	6.02	6.16	2.93	2.72	0.46
KIAA1199	KIAA1199 (KIAA1199)	7080	116.42	121.66	61.32	58.71	0.51
FAM43A	family with sequence similarity 43, member A (FAM43A)	3182	5.57	5.98	3.25	2.92	0.53
IL8	interleukin 8 (IL8)	1718	47.25	46.91	24.02	27.43	0.55
NOV	nephroblastoma overexpressed gene (NOV)	2601	6.98	7.15	3.66	4.21	0.56
DPT	dermatopontin (DPT)	1749	13.08	13.19	7.41	7.65	0.57
GRPR	gastrin-releasing peptide receptor (GRPR)	2681	5.95	5.43	3.32	3.73	0.62
PENK	proenkephalin (PENK)	1354	11.59	12.16	7.58	7.24	0.63
CHRM2	cholinergic receptor, muscarinic 2 (CHRM2)	2782	4.77	4.6	2.87	3.05	0.63
SULF1	sulfatase 1 (SULF1)	5716	199.34	192.14	123.73	129.58	0.65
SMOX	spermine oxidase (SMOX)	2203	7.96	8.23	5.58	4.97	0.65
WISP2	WNT1 inducible signaling pathway protein 2 (WISP2)	1433	4.45	4.91	3.33	2.85	0.66
PODN	podocan (PODN)	3417	17.56	17.96	13.06	10.92	0.68
PCDH10	protocadherin 10 (PCDH10)	5384	10.29	10.69	7.08	7.13	0.68
CEBPD	CCAAT/enhancer binding protein (C/EBP), delta (CEBPD)	1269	7.05	6.92	4.89	4.56	0.68
NTM	neurotrimin (NTM)	3408	4.56	4.42	2.96	3.15	0.68
SIPA1L2	signal-induced proliferation-associated 1 like 2 (SIPA1L2)	6501	7.29	7.08	5.07	4.79	0.68
GABBR2	gamma-aminobutyric acid (GABA) B receptor, 2 (GABBR2)	5802	4.88	4.86	3.47	3.25	0.69
FGF7	fibroblast growth factor 7 (FGF7)	3936	13.62	13.75	8.83	10.06	0.69
MMP1	matrix metalloproteinase 1 (interstitial collagenase) (MMP1)	2081	66.28	67.05	44.15	47.73	0.69
CLDN11	claudin 11 (CLDN11)	2761	136.63	138.87	96.23	94.59	0.69
NAMPT	nicotinamide phosphoribosyltransferase (NAMPT)	4593	16.11	16.92	10.67	12.29	0.69
OSR1	odd-skipped related 1 (Drosophila) (OSR1)	1911	7.67	7.46	5.19	5.31	0.69
AKAP12	A kinase (PRKA) anchor protein 12 (AKAP12)	8450	14.13	14.41	9.9	10.12	0.70
ELOVL4	elongation of very long chain fatty acids (FEN1/Elo2, SUR4/Elo3, yeast)-like 4 (ELOVL4)	3085	4.08	3.95	2.71	2.92	0.70
WNT5A	wingless-type MMTV integration site family, member 5A (WNT5A)	5855	37.53	36.39	25.64	26.7	0.71
SERPINB2	serpin peptidase inhibitor, clade B (ovalbumin), member 2 (SERPINB2)	2180	84.68	84.81	58.93	61.97	0.71
TFPI2	tissue factor pathway inhibitor 2 (TFPI2)	1203	55.81	54.92	38.76	40.73	0.72
AMIGO2	adhesion molecule with Ig-like domain 2 (AMIGO2)	3849	5.12	4.99	3.52	3.79	0.72
FZD8	frizzled homolog 8 (Drosophila) (FZD8)	3186	4.24	4.23	3.37	2.77	0.72
APCDD1	adenomatosis polyposis coli down-regulated 1 (APCDD1)	2579	5.51	5.34	4.08	3.81	0.72
CXCL3	chemokine (C-X-C motif) ligand 3 (CXCL3)	1166	4.04	4.04	2.79	3.1	0.73
GREM2	gremlin 2 (GREM2)	4199	15.68	16.02	11.42	11.69	0.73
CDC42EP2	CDC42 effector protein (Rho GTPase binding) 2 (CDC42EP2)	2001	16.01	17.99	13.56	11.44	0.74
SGK1	serum/glucocorticoid regulated kinase 1 (SGK1)	3208	25.31	24.65	17.78	18.83	0.74
PTGER3	prostaglandin E receptor 3 (subtype EP3) (PTGER3)	7759	4.1	4.27	3.03	3.18	0.74
CNIH3	cornichon homolog 3 (Drosophila) (CNIH3)	2372	3.93	4.62	3.04	3.33	0.75
THBS2	thrombospondin 2 (THBS2)	5826	22.06	22.43	16.7	16.38	0.75
IER3	immediate early response 3 (IER3)	1254	41.08	45.51	32.45	32.63	0.75
BCL6	B-cell CLL/lymphoma 6 (BCL6)	3662	5.99	6.29	4.72	4.52	0.75
WNT2	wingless-type MMTV integration site family member 2 (WNT2)	2907	5.39	5.6	4.18	4.11	0.75
NR4A1	nuclear receptor subfamily 4, group A, member 1 (NR4A1)	2692	3.24	3.67	3	2.2	0.75
UCHL1	ubiquitin carboxyl-terminal esterase L1 (ubiquitin thiolesterase) (UCHL1)	1141	20.78	21.7	15.12	17.07	0.76
NID2	nidogen 2 (osteonidogen) (NID2)	5063	4.71	4.81	3.71	3.55	0.76
AHR	aryl hydrocarbon receptor (AHR)	6247	14.24	13.98	10.2	11.41	0.76
ITGA11	integrin, alpha 11 (ITGA11)	5035	25.48	25.53	19.72	19.08	0.76
FAM101B	family with sequence similarity 101, member B (FAM101B)	3895	109.64	109.18	83.59	84.97	0.77
MC4R	melanocortin 4 receptor (MC4R)	1438	6.75	7.45	5.36	5.56	0.77
NTN4	netrin 4 (NTN4)	3634	22.93	24.36	17.84	18.43	0.77
SEMA5A	sema domain, seven thrombospondin repeats (type 1 and type 1-like), transmembrane domain (TM) and short cytoplasmic domain, (semaphorin) 5A (SEMA5A)	11825	13.53	13.13	10.16	10.33	0.77
SOCS3	suppressor of cytokine signaling 3 (SOCS3)	2746	12.34	12.48	10.09	9.09	0.78
TRPC4	transient receptor potential cation channel, subfamily C, member 4 (TRPC4)	3549	10.66	10.44	8.22	8.13	0.78
LIN7A	lin-7 homolog A (C. elegans) (LIN7A)	1235	11.08	10.35	8.3	8.33	0.78
OLFM2	olfactomedin 2 (OLFM2)	1899	8.42	7.41	6.05	6.23	0.78
ZNF521	zinc finger protein 521 (ZNF521)	4985	4.78	4.56	3.68	3.57	0.78
SECTM1	secreted and transmembrane 1 (SECTM1)	2282	9.25	9.59	8.08	6.57	0.78
SCIN	scinderin (SCIN)	3261	8.96	9.27	7.09	7.05	0.78
BEX1	brain expressed, X-linked 1 (BEX1)	862	6.48	6.84	5.32	5.05	0.78
LOXL3	lysyl oxidase-like 3 (LOXL3)	3121	8.95	8.86	7.4	6.48	0.78
AP1S2	adaptor-related protein complex 1, sigma 2 subunit (AP1S2)	2283	40.62	37	29.09	31.71	0.78
EPGN	epithelial mitogen homolog (mouse) (EPGN)	847	7.58	8.43	6.27	6.25	0.78
CDH2	cadherin 2, type 1, N-cadherin (neuronal) (CDH2)	4380	61.45	60.75	46.66	49.87	0.79
STC2	stanniocalcin 2 (STC2)	5361	147.21	159.34	122.53	119.47	0.79
ICAM3	intercellular adhesion molecule 3 (ICAM3)	1796	5.01	5.57	4.54	3.88	0.79

LUM	lumican (LUM)	2116	254.75	245.27	191.91	203.53	0.79
PVRL3	poliovirus receptor-related 3 (PVRL3)	1650	48.55	47.07	37.3	38.6	0.79
CPXM2	carboxypeptidase X (M14 family), member 2 (CPXM2)	3750	7.61	7.76	5.94	6.26	0.79
CCRL1	chemokine (C-C motif) receptor-like 1 (CCRL1)	2402	7.04	6.57	5.39	5.4	0.79
FAM198B	family with sequence similarity 198, member B (FAM198B)	4854	5.06	5.37	3.95	4.32	0.79
MAMLD1	mastermind-like domain containing 1 (MAMLD1)	4608	13.1	12.89	10.76	9.9	0.79
ELTD1	EGF, latrophilin and seven transmembrane domain containing 1 (ELTD1)	3619	8.31	8.07	6	7	0.79
LMCD1	LIM and cysteine-rich domains 1 (LMCD1)	1754	12.74	13.2	10.66	9.89	0.79
KIAA1644	KIAA1644 (KIAA1644)	6741	3.83	4.08	3.17	3.1	0.79
TMEM200A	transmembrane protein 200A (TMEM200A)	5042	20.07	19.61	15.03	16.61	0.80
FAM58B	family with sequence similarity 58, member B (FAM58B)	988	3.23	3.4	2.88	2.41	0.80
USP53	ubiquitin specific peptidase 53 (USP53)	6612	11.78	11.32	8.75	9.71	0.80
CHAC1	ChaC, cation transport regulator homolog 1 (E. coli) (CHAC1)	1578	9.65	11.15	9.27	7.37	0.80
SLC38A1	solute carrier family 38, member 1 (SLC38A1)	8487	16.47	16.37	12.76	13.56	0.80
ADM	adrenomedullin (ADM)	1449	120.06	124.17	101.53	94.65	0.81
SLC16A7	solute carrier family 16, member 7 (monocarboxylic acid transporter 2) (SLC16A7)	3575	11.88	11.05	8.8	9.63	0.81
GREM1	gremlin 1 (GREM1)	4150	1089.4	1089.2	846.71	912.42	0.81
RUNX2	runt-related transcription factor 2 (RUNX2)	5720	3.23	3.05	2.36	2.7	0.81
DHRS3	dehydrogenase/reductase (SDR family) member 3 (DHRS3)	1825	21.89	21.67	18.48	16.65	0.81
CREB3L1	cAMP responsive element binding protein 3-like 1 (CREB3L1)	2702	144.27	134.87	120.33	105.79	0.81
C10orf125	chromosome 10 open reading frame 125 (C10orf125)	768	3.94	3.78	3.41	2.89	0.81
CXCL2	chemokine (C-X-C motif) ligand 2 (CXCL2)	1234	3.47	3.26	2.76	2.73	0.81
PDGFRA	platelet-derived growth factor receptor, alpha polypeptide (PDGFRA)	6574	48.74	47.67	38.28	39.81	0.81
SNAI1	snail homolog 1 (Drosophila) (SNAI1)	1722	6.55	6.16	5.3	5.04	0.81
CCL2	chemokine (C-C motif) ligand 2 (CCL2)	760	8.79	9.09	6.91	7.57	0.81
CTHRC1	collagen triple helix repeat containing 1 (CTHRC1)	1236	4.26	4.51	3.35	3.79	0.81
NFIL3	nuclear factor, interleukin 3 regulated (NFIL3)	2104	11.66	11.73	9.43	9.74	0.82
TNFRSF21	tumor necrosis factor receptor superfamily, member 21 (TNFRSF21)	3662	3.7	3.55	3.08	2.84	0.82
S1PR2	sphingosine-1-phosphate receptor 2 (S1PR2)	3589	5.99	5.63	5.08	4.47	0.82
ADM2	adrenomedullin 2 (ADM2)	4246	5.51	5.43	4.85	4.1	0.82
FAM46A	family with sequence similarity 46, member A (FAM46A)	5617	28.26	27.49	22.24	23.38	0.82
LYPD6	LY6/PLAUR domain containing 6 (LYPD6)	4111	10.32	9.35	7.74	8.43	0.82
ENPP1	ectonucleotide pyrophosphatase/phosphodiesterase 1 (ENPP1)	7442	6.6	5.99	5.03	5.28	0.82
ZDHHC14	zinc finger, DHHC-type containing 14 (ZDHHC14)	2821	4.35	4.06	3.66	3.22	0.82
GREB1L	growth regulation by estrogen in breast cancer-like (GREB1L)	6052	3.42	3.19	2.89	2.53	0.82
PRDM1	PR domain containing 1, with ZNF domain (PRDM1)	5165	4.27	4.28	3.66	3.34	0.82
MKX	mohawk homeobox (MKX)	3658	16.97	16.57	13.35	14.48	0.83
IRS1	insulin receptor substrate 1 (IRS1)	8743	8.85	9.18	7.57	7.35	0.83
NNMT	nicotinamide N-methyltransferase (NNMT)	1579	40.61	42.51	35.69	32.85	0.83
COLEC12	collectin sub-family member 12 (COLEC12)	3134	43.39	41.42	35.36	34.91	0.83
ETHE1	ethylmalonic encephalopathy 1 (ETHE1), nuclear gene encoding mitochondrial protein	978	48.35	52.76	45.23	38.61	0.83
DUSP6	dual specificity phosphatase 6 (DUSP6)	2842	5.84	5.53	5.04	4.36	0.83
TUBA3C	tubulin, alpha 3c (TUBA3C)	1564	5.67	5.23	4.61	4.42	0.83
PSG1	pregnancy specific beta-1-glycoprotein 1 (PSG1)	2306	6.96	7.15	5.73	5.94	0.83
PID1	phosphotyrosine interaction domain containing 1 (PID1)	2837	5.05	5.02	3.93	4.42	0.83
ABLIM3	actin binding LIM protein family, member 3 (ABLIM3)	4335	11.96	11.91	10.52	9.22	0.83
CCDC75	coiled-coil domain containing 75 (CCDC75)	1257	7.53	6	5.2	6.09	0.83
MON1A	MON1 homolog A (yeast) (MON1A)	2244	6.9	7.05	6.31	5.32	0.83
LAMB3	laminin, beta 3 (LAMB3)	4339	4.78	4.95	4.46	3.67	0.83
TMEM158	transmembrane protein 158 (gene/pseudogene) (TMEM158)	1876	9.33	10.51	8.87	7.67	0.83
UPP1	uridine phosphorylase 1 (UPP1)	1857	7.97	7.8	7.18	5.92	0.83
SVIL	supervillin (SVIL)	8306	4.9	4.93	4.09	4.07	0.83
HIST1H2AB	histone cluster 1, H2ab (HIST1H2AB)	477	4.12	4.3	3.6	3.43	0.83
CYP27A1	cytochrome P450, family 27, subfamily A, polypeptide 1 (CYP27A1), nuclear gene encoding mitochondrial protein	2388	4.51	4.68	4.11	3.56	0.83
DPP4	dipeptidyl-peptidase 4 (DPP4)	3913	42.1	40.05	33.24	35.05	0.83
C8orf38	chromosome 8 open reading frame 38 (C8orf38), nuclear gene encoding mitochondrial protein	1808	4.5	4.53	3.73	3.8	0.83
SLC7A11	solute carrier family 7, (cationic amino acid transporter, y+ system) member 11 (SLC7A11)	9648	21.71	21.43	16.71	19.1	0.83
IFITM1	interferon induced transmembrane protein 1 (9-27) (IFITM1)	733	70.84	66.86	60.31	54.42	0.83
INHBA	inhibin, beta A (INHBA)	2175	59.16	59.08	48.68	49.78	0.83
C1orf85	chromosome 1 open reading frame 85 (C1orf85)	1603	32.17	32.2	28.48	25.34	0.83
PLEKHF1	pleckstrin homology domain containing, family F (with FYVE domain) member 1 (PLEKHF1)	1774	3.26	3.92	2.97	3.02	0.83
PRICKLE3	prickle homolog 3 (Drosophila) (PRICKLE3)	1990	4.18	4.01	3.75	3.06	0.83
VLDLR	very low density lipoprotein receptor (VLDLR)	3646	3.93	3.6	2.97	3.3	0.83
C20orf177	chromosome 20 open reading frame 177 (C20orf177)	5119	3.14	3.28	2.43	2.92	0.83
COL14A1	collagen, type XIV, alpha 1 (COL14A1)	6463	4.09	3.88	3.4	3.26	0.83

Supplementary Data File 1.

Nanostring data and calculations for 32-gene CdLS lymphoblastoid expression profiling

(Microsoft Excel file).

Supplementary Data Files 2-5.

High resolution images of data from immunoblotting experiments. Uncompressed original files can be viewed at <http://www.iam.u-tokyo.ac.jp/chromosomeinformatics/supplemental/index.html>.

Supplementary References

1. Balasubramanian, S. et al. A novel histone deacetylase 8 (HDAC8)-specific inhibitor PCI-34051 induces apoptosis in T-cell lymphomas. *Leukemia* **22**, 1026-34 (2008).
2. Hubner, N.C. et al. Re-examination of siRNA specificity questions role of PICH and Tao1 in the spindle checkpoint and identifies Mad2 as a sensitive target for small RNAs. *Chromosoma* **119**, 149-65 (2010).
3. Westhorpe, F.G., Diez, M.A., Gurden, M.D., Tighe, A. & Taylor, S.S. Re-evaluating the role of Tao1 in the spindle checkpoint. *Chromosoma* **119**, 371-9 (2010).
4. Carrel, L. & Willard, H.F. X-inactivation profile reveals extensive variability in X-linked gene expression in females. *Nature* **434**, 400-4 (2005).
5. Ng, P.C. & Henikoff, S. SIFT: Predicting amino acid changes that affect protein function. *Nucleic Acids Res* **31**, 3812-4 (2003).
6. Sunyaev, S. et al. Prediction of deleterious human alleles. *Hum Mol Genet* **10**, 591-7 (2001).
7. Liu, J. et al. Transcriptional dysregulation in NIPBL and cohesin mutant human cells. *PLoS Biol* **7**, e1000119 (2009).
8. Wendt, K.S. et al. Cohesin mediates transcriptional insulation by CCCTC-binding factor. *Nature* **451**, 796-801 (2008).
9. Stedman, W. et al. Cohesins localize with CTCF at the KSHV latency control region and at cellular c-myc and H19/lgf2 insulators. *Embo J* **27**, 654-66 (2008).
10. Parelho, V. et al. Cohesins functionally associate with CTCF on mammalian chromosome arms. *Cell* **132**, 422-33 (2008).
11. Dorsett, D. Cohesin, gene expression and development: lessons from Drosophila. *Chromosome Res* **17**, 185-200 (2009).
12. Muto, A., Calof, A.L., Lander, A.D. & Schilling, T.F. Multifactorial origins of heart and gut defects in nipbl-deficient zebrafish, a model of Cornelia de Lange Syndrome. *PLoS Biol* **9**, e1001181 (2011).
13. Kawauchi, S. et al. Multiple organ system defects and transcriptional dysregulation in the Nipbl(+/-) mouse, a model of Cornelia de Lange Syndrome. *PLoS Genet* **5**, e1000650 (2009).
14. Waizenegger, I.C., Hauf, S., Meinke, A. & Peters, J.M. Two distinct pathways remove mammalian cohesin from chromosome arms in prophase and from centromeres in anaphase. *Cell* **103**, 399-410 (2000).
15. Hauf, S., Waizenegger, I.C. & Peters, J.M. Cohesin cleavage by separase required for anaphase and cytokinesis in human cells. *Science* **293**, 1320-3 (2001).
16. Beckouet, F. et al. An Smc3 acetylation cycle is essential for establishment of sister chromatid cohesion. *Mol Cell* **39**, 689-99 (2010).
17. Borges, V. et al. Hos1 deacetylates Smc3 to close the cohesin acetylation cycle. *Mol Cell* **39**, 677-88 (2010).
18. Xiong, B., Lu, S. & Gerton, J.L. Hos1 is a lysine deacetylase for the Smc3 subunit of cohesin. *Curr Biol* **20**, 1660-5 (2010).
19. Unal, E. et al. A molecular determinant for the establishment of sister chromatid cohesion. *Science* **321**, 566-9 (2008).
20. Witt, O., Deubzer, H.E., Milde, T. & Oehme, I. HDAC family: What are the cancer relevant targets? *Cancer Lett* **277**, 8-21 (2009).
21. Williams, S.R. et al. Haploinsufficiency of HDAC4 causes brachydactyly mental retardation syndrome, with brachydactyly type E, developmental delays, and behavioral problems. *Am J Hum Genet* **87**, 219-28 (2010).
22. Haberland, M., Mokalled, M.H., Montgomery, R.L. & Olson, E.N. Epigenetic control of skull morphogenesis by histone deacetylase 8. *Genes Dev* **23**, 1625-30 (2009).
23. Bausch, C. et al. Transcription alters chromosomal locations of cohesin in *Saccharomyces cerevisiae*. *Mol Cell Biol* **27**, 8522-32 (2007).
24. Lengronne, A. et al. Cohesin relocation from sites of chromosomal loading to places of convergent transcription. *Nature* **430**, 573-8 (2004).